Cell

Coding Region Polyadenylation Generates a Truncated tRNA Synthetase that Counters Translation Repression

Peng Yao,[1] Alka A. Potdar,[1,6] Abul Arif,[1] Partho Sarothi Ray,[1,3] Rupak Mukhopadhyay,[1,4] Belinda Willard,[2] Yichi Xu,[5] Jun Yan,[5] Gerald M. Saidel,[6,7] and Paul L. Fox[1,*]
[1]Department of Cell Biology
[2]Mass Spectrometry Laboratory for Protein Sequencing
The Lerner Research Institute, Cleveland Clinic, Cleveland, OH 44195, USA
[3]Department of Biological Sciences, Indian Institute of Science Education and Research, Kolkata 700 064, India
[4]Department of Molecular Biology and Biotechnology, Tezpur University, Tezpur, Sonitpur, Assam-784 028, India
[5]CAS-MPG Partner Institute for Computational Biology, Shanghai Institute for Biological Sciences, Chinese Academy of Sciences, Shanghai 200031, China
[6]Department of Biomedical Engineering
[7]Center for Modeling Integrated Metabolic Systems
Case Western Reserve University, Cleveland, OH 44106, USA
*Correspondence: foxp@ccf.org
DOI 10.1016/j.cell.2012.02.018

SUMMARY

Posttranscriptional regulatory mechanisms superimpose "fine-tuning" control upon "on-off" switches characteristic of gene transcription. We have exploited computational modeling with experimental validation to resolve an anomalous relationship between mRNA expression and protein synthesis. The GAIT (*g*amma-interferon-*a*ctivated *i*nhibitor of *t*ranslation) complex repressed VEGF-A synthesis to a low, constant rate independent of *VEGF-A* mRNA expression levels. Dynamic model simulations predicted an inhibitory GAIT-element-interacting factor to account for this relationship and led to the identification of a truncated form of glutamyl-prolyl tRNA synthetase (EPRS), a GAIT constituent that mediates binding to target transcripts. The truncated protein, $EPRS^{N1}$, shields GAIT-element-bearing transcripts from the inhibitory GAIT complex, thereby dictating a "translational trickle" of GAIT target proteins. $EPRS^{N1}$ mRNA is generated by polyadenylation-directed conversion of a Tyr codon in the *EPRS*-coding sequence to a stop codon (PAY*). Genome-wide analysis revealed multiple candidate PAY* targets, including the authenticated target *RRM1*, suggesting a general mechanism for production of C terminus-truncated regulatory proteins.

INTRODUCTION

The human genome encodes about 25,000 mRNAs that represent a lower bound of the expressed proteome in eukaryotic organisms due to expansion from upstream open reading frames (ORFs), alternative splicing, alternative polyadenylation, post-translational modification, and proteolysis. Alternative protein forms can acquire completely distinct activities but more commonly exhibit a function related to the parental forms. One major protein family featuring a plethora of alternative structures and functions are the eukaryotic aminoacyl-tRNA synthetases (AARS). AARS are constitutive "house-keeping" enzymes, ubiquitous in the three kingdoms of life, and required for activation of cognate amino acids for interpretation of the genetic code (Ibba and Söll, 2000; Ribas de Pouplana and Schimmel, 2001). In addition to this ancient function, newly evolved noncanonical functions of multiple metazoan AARS depend on domains recently (in terms of evolutionary time) appended to the enzyme catalytic cores (Guo et al., 2010; Park et al., 2008). In previous studies of translational control of gene expression, we have shown that the bifunctional AARS glutamyl-prolyl tRNA synthetase (EPRS) exhibits an additional noncanonical function that is similarly dependent on a metazoa-specific appended domain (Mukhopadhyay et al., 2009; Ray et al., 2011).

IFN-γ treatment of myeloid cells robustly induces ceruloplasmin (*Cp*) and vascular endothelial growth factor-A (*VEGF-A*) mRNAs. However, synthesis of the proteins stops almost completely about 14–16 hr after IFN-γ treatment, despite undiminished mRNA level (Mazumder and Fox, 1999; Ray and Fox, 2007). Translational silencing requires binding of the GAIT (*g*amma-interferon-*a*ctivated *i*nhibitor of *t*ranslation) complex, consisting of EPRS as well as ribosomal protein L13a, NS1-associated protein 1 (NSAP1), and glyceraldehyde 3-phosphate dehydrogenase (GAPDH), to structural elements in the target mRNA 3′ untranslated regions (UTRs) (Mazumder and Fox, 1999; Sampath et al., 2003) (Figure 1A). GAIT complex assembly is driven by IFN-γ-inducible phosphorylation of EPRS and L13a and consequent release from their parent macromolecular complexes, notably the aminoacyl-tRNA multisynthetase complex

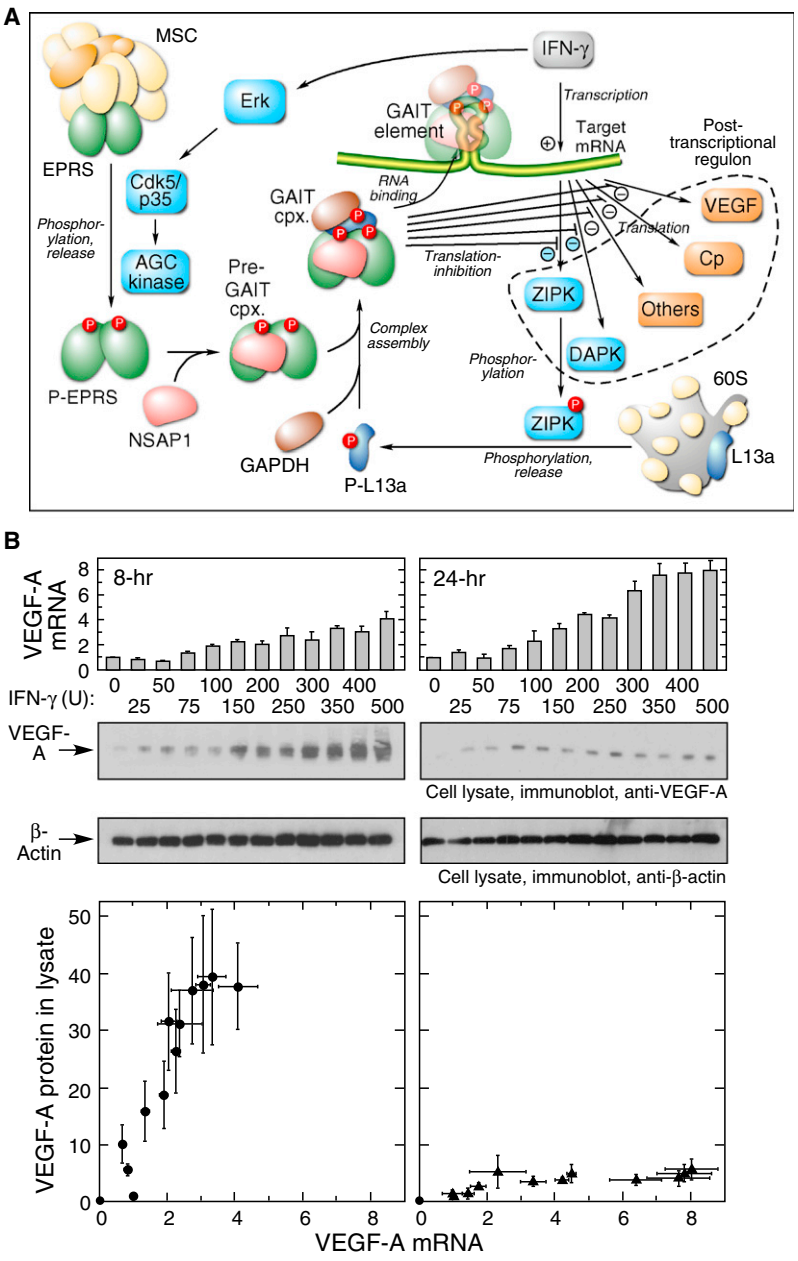

Figure 1. Differential Regulation of VEGF-A mRNA and Protein by the GAIT Pathway

(A) Schematic of GAIT pathway of transcript-selective translational control.

(B) IFN-γ-stimulated monocytic cells maintain low-level expression of VEGF-A. U937 cells were treated with IFN-γ at up to 500 U/ml for 8 (left) or 24 (right) hr. *VEGF-A* mRNA was determined by qRT-PCR (top), and VEGF-A protein and β-actin in cell lysates by immunoblot analysis (middle panels). VEGF-A protein as function of *VEGF-A* mRNA is shown (mean ± standard error of the mean [SEM], n = 3) (bottom).

(MSC) (Arif et al., 2009, 2011; Sampath et al., 2004) and the large ribosomal subunit, respectively (Mazumder et al., 2003; Mukhopadhyay et al., 2008). Assembly occurs in two stages. During the first 2 hr period, phospho-EPRS binds NSAP1 to form an inactive, pre-GAIT complex that does not bind GAIT-bearing target mRNA. About 12–14 hr later, phospho-L13a and GAPDH join the pre-GAIT complex to form the heterotetrameric GAIT complex that binds the 3′ UTR GAIT element of target mRNAs and blocks translation initiation (Kapasi et al., 2007; Mazumder et al., 2001).

EPRS has a special role in GAIT-mediated translational control, as it is solely responsible for recognition and interaction with GAIT elements in target mRNAs (Ray et al., 2009; Sampath et al., 2004). Metazoan EPRS is the only bifunctional AARS and catalyzes Glu and Pro ligation to cognate tRNAs (Ray et al., 2011). Human EPRS is a 172 kDa, 1512 amino acid polypeptide consisting of three major domains. The N and C termini contain ERS and PRS catalytic domains, respectively, joined by a 300 amino acid linker containing three tandem WHEP-TRS (referred to as WHEP) domains. The WHEP domain is a 50 amino acid helix-turn-helix structure (Cahuzac et al., 2000; Jeong et al., 2000) named after the AARS containing them, i.e., *W*RS, *H*RS, and *EP*RS. The upstream WHEP repeat pair is essential for high-affinity binding to the GAIT RNA element, whereas the overlapping, downstream pair (and adjacent spacers) contains the phosphorylation sites essential for GAIT complex assembly (Jia et al., 2008).

L13a phosphorylation is a critical event determining the timing of GAIT system activation (Figure 1A). IFN-γ induces L13a phosphorylation by activation of a kinase cascade in which death-associated protein kinase-1 (DAPK) activates the proximal kinase zipper-interacting protein kinase (ZIPK) (Mukhopadhyay et al., 2008). *DAPK* and *ZIPK* mRNAs contain functional 3′ UTR GAIT elements, and thus the inhibitory pathway activated by the kinases also suppresses their expression. Delayed feedback inhibition of DAPK and ZIPK restores the cell to the basal state and allows GAIT system reactivation by subsequent stimulation.

Here we exploit a dynamic modeling approach to understand the mechanism underlying a marked discrepancy in expression of GAIT system targets. Activation of monocytic cells for 24 hr by a wide range of concentrations of IFN-γ induces an equally broad range of expression of *VEGF-A* mRNA; however, differential mRNA expression does not correspond to differential protein expression but rather to a constant, low-level "trickle" of synthesis of VEGF-A protein. Mathematical modeling of the known features of the GAIT system failed to replicate these observations. But the addition of a putative GAIT-element-interacting factor (GEIF) to the model permitted a successful fit. The modeling was validated by discovery of a novel truncated *EPRS* mRNA and protein responsible for the observed aberrant

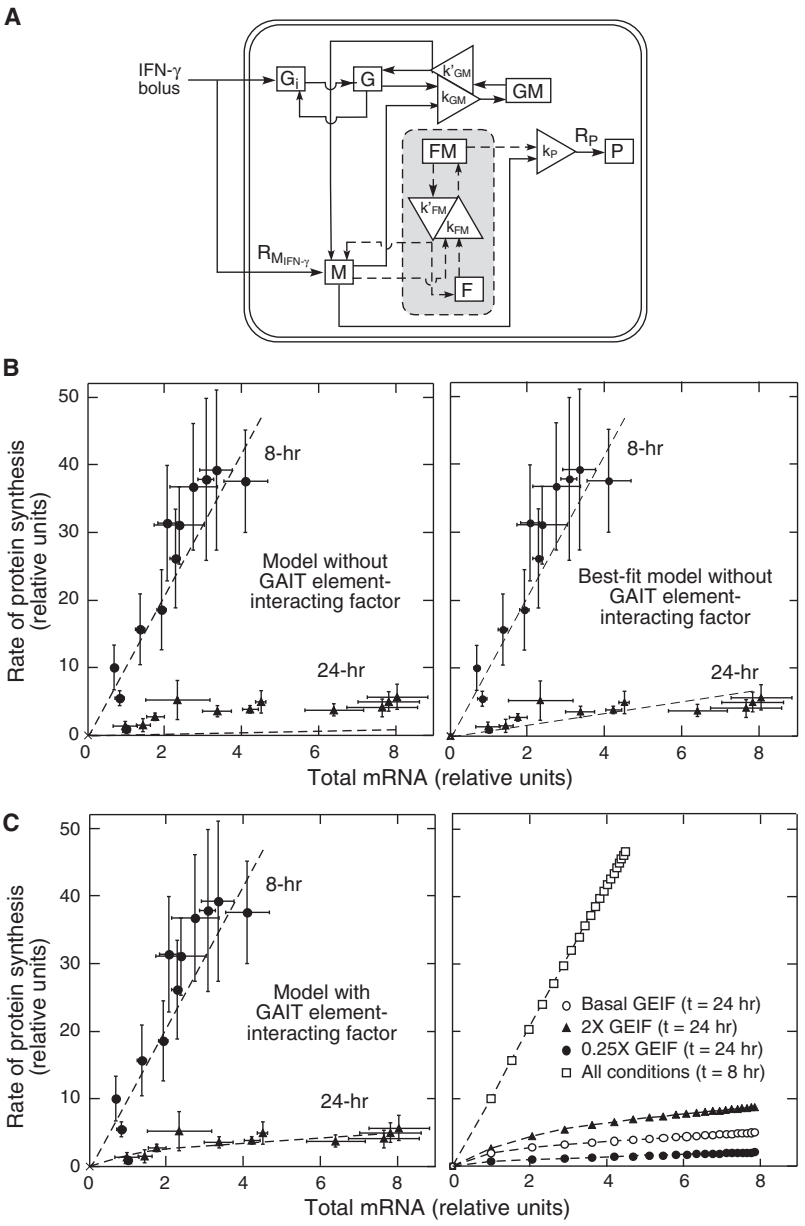

Figure 2. Dynamic Modeling of GAIT System Indicates that GEIF Is Responsible for the Translational Trickle of VEGF-A Expression

(A) Dynamic modeling of GAIT system. Key model features are as follows: G_i, inactive (or unformed) GAIT complex; G, active GAIT complex; M, GAIT-element-bearing mRNA; GM, GAIT complex-bound mRNA; P, newly synthesized GAIT target protein. Dashed compartment contains the following: F, GEIF; FM, GEIF-bound mRNA. Rate constants are indicated within triangles.

(B) Model simulations without GEIF. Rate of protein synthesis versus total mRNA before (8 hr) and after (24 hr) translational silencing using the initial model without GEIF (dashed lines); model simulations were done for a range of IFN-γ concentrations (left). Model simulations are with best-fit ratio of GAIT complex to target mRNA (ratio = 15) as determined by nonlinear regression (right).

(C) Model simulations with GEIF. Simulations (dashed lines and curves) in presence of GEIF are based on experimentally determined parameters (left) and in presence of a 2-fold higher or 75% lower amount of GEIF (right).

See also Figure S1 and Tables S1 and S2.

relationship between *VEGF-A* mRNA and protein expression. Moreover, we have elucidated an RNA-processing mechanism that generates the truncated *EPRS* mRNA and protein and contributes to transcriptome expansion.

RESULTS

Dynamic Modeling of GAIT System Predicts a GAIT-Element-Interacting Factor

During investigation of GAIT response dynamics, a dose-response experiment revealed an unexpected result. U937 monocytic cells were treated with a broad range of concentrations of IFN-γ for 8 hr, a time before induction of GAIT-mediated silencing activity, and for 24 hr, when GAIT silencing activity is in effect. At 8 hr, an increase in IFN-γ was associated with an increase of both *VEGF-A* mRNA and lysate protein (a relative measure of the rate of synthesis of the secreted protein) (Figure 1B, left), and a near-linear relationship between *VEGF-A* mRNA and protein synthesis was observed. In contrast, at 24 hr, VEGF-A protein was expressed at a low, near-constant amount over a wide range of IFN-γ treatment that was independent of the high, variable *VEGF-A* mRNA expression (Figure 1B, right).

To understand the mechanism underlying this "translational trickle" of GAIT target protein expression observed at 24 hr, an initial mathematical model of the system dynamics containing the key components that regulate gene expression was developed. This mechanism-based model included delayed activation of the GAIT complex after 14 hr and feedback inhibition of DAPK and ZIPK after 32 hr (Figure 2A, without dashed compartment and vectors). Complete model details, initial conditions (Table S1 available online), and parameters (Table S2) are described in Modeling Procedures in the Extended Experimental Procedures. The maximum amount of GAIT complex formed was determined by the amount of free L13a in cells treated with IFN-γ for 24 hr, previously shown to be about 95% of total L13a (Mazumder et al., 2003). Total GAIT-element-bearing target mRNA under the same condition was approximated by RNA immunoprecipitation (RIP) with anti-EPRS antibody. The ratio of GAIT complex to total target mRNA is about 50–100 in U937 cells, and the upper limit value of 100 was used for model simulation. The kinetics and dose response of *VEGF-A* mRNA and protein following IFN-γ stimulation were taken as representative of GAIT targets as a whole. The model rate equations were represented by ordinary differential equations, and simulated results

were compared to the experimental measurements. The simulation gave a linear relationship between target protein synthesis rate and mRNA at both 8 and 24 hr; moreover, protein synthesis at 24 hr was repressed almost completely (Figure 2B, left). When the ratio of GAIT complex to target mRNA was varied (to influence the extent of silencing), the model still could not simulate the experimental nonlinear relationship between total mRNA and protein synthesis rate. The best-fit value for the GAIT complex-to-target mRNA ratio was calculated by least-squares fitting of the model output to the experimental data. Although the fit was improved, the model failed to predict the observed nonlinear relationship between VEGF-A mRNA and protein synthesis rate (Figure 2B, right).

We considered the potential role of a GAIT complex inhibitor that sequesters the complex from target mRNAs, but this model also generated a linear relationship between VEGF-A mRNA and protein synthesis rate at 24 hr (Figures S1A–S1D). Likewise, a model featuring two inducible pools of mRNA with and without the GAIT element failed to simulate the nonlinear relationship (Figures S1E and S1F). Finally, we considered the possibility of a GEIF that binds GAIT-element-bearing mRNAs and prevents their interaction with the GAIT complex while permitting translation (Figure 2A, with dashed compartment and vectors). Upon inclusion of GEIF in an enhanced model, simulation produced the experimentally observed nonlinear relationship between protein synthesis rate and mRNA at 24 hr, although maintaining the linear relationship at 8 hr (Figure 2C, left). The species dynamics indicate the distribution of GAIT-element-bearing mRNAs between the GAIT complex-bound, GEIF-bound, and unbound forms (Figure S1G). The small amount of GEIF-bound, protected mRNA directs a constant "translational trickle" at 24 hr. Nonlinear regression of the experimental data with the GEIF-containing model gave estimates of stoichiometry and dissociation constant of this putative binding factor (Table S2). We compared the squared residual (deviation of simulated protein synthesis rate from the experimental measurement) for various IFN-γ_0 inputs for several models. The best-fitting model, as indicated by the minimum value of the sum of squared residuals, was obtained for the enhanced model with GEIF (Figure S1H). A p value > 0.05 indicates no statistical difference between the model and experimental outputs, i.e., a good model fit. The enhanced model with GEIF ($p = 0.23$) satisfied this criterion, whereas the best-fit model without GEIF ($p = 0.002$) did not (see Extended Experimental Procedures for details). Increasing the amount of GEIF in the model increased the steady-state trickle level, whereas decreasing GEIF had the opposite effect (Figure 2C, right).

Discovery of a Truncated EPRS Variant Containing Only the Upstream WHEP Domain Pair that Binds the GAIT Element

To determine the nature of the putative GEIF, i.e., RNA or protein, we examined whether expression of a second GAIT mRNA target exhibits similar dynamic characteristics. *ZIPK* mRNA contains a GAIT element with a predicted secondary structure similar to that of *VEGF-A* mRNA but with a completely unrelated primary sequence (Mukhopadhyay et al., 2008). U937 cells were treated with IFN-γ for 8 and 24 hr and *ZIPK* mRNA determined by RT-PCR and protein synthesis by [^{35}S]methionine labeling followed by immunoprecipitation. The relationship between *ZIPK* mRNA expression and protein synthesis was similar to that observed for *VEGF-A* (Figure 3A). The experimentally determined GAIT elements of *VEGF-A* and *ZIPK* have completely different mRNA sequences but nearly identical calculated secondary structures (Mukhopadhyay et al., 2008; Ray and Fox, 2007). Thus the putative factor responsible for binding both elements is unlikely to be a sequence-specific microRNA (or other noncoding RNA) but rather an RNA-binding protein that recognizes the GAIT structural element common to all GAIT target mRNAs. Moreover, these results suggest that GEIF-directed relief of translational silencing might represent an additional layer of posttranscriptional regulation of the GAIT regulon.

To explore experimentally the presence of a GEIF, we considered previous studies showing that the upstream pair of WHEP domains in the EPRS linker is sufficient for high-affinity binding to the GAIT RNA element but does not contain the phosphorylation sites required for interaction with GAIT constituents (Arif et al., 2009; Jia et al., 2008). These findings suggest that a minor EPRS variant containing only the upstream pair of WHEP domains might be responsible for the observed trickle phenomenon. An approximately 95 kDa EPRS variant was detected in lysates from human monocytic U937 cells (Figure 3B) and from primary human peripheral blood monocytes (PBM, Figure 3C) by immunoblot with antibody against the EPRS linker domain. Anti-N-terminus antibody also detected both proteins, but PRS-specific antibody recognized only full-length EPRS. The N terminus-containing truncated form (designated EPRS^{N1}) was analyzed by mass spectrometry following immunoprecipitation with anti-linker antibody and SDS-PAGE. Peptide coverage spanned ERS and the first two of three WHEP repeats in the linker domain (Figure 3D).

To investigate the mechanism underlying expression of truncated EPRS, total RNA from U937 cells was subjected to northern analysis with region-specific cDNA probes. Major 5.5 kb and minor 3 kb bands were detected with an ERS-specific probe, but the smaller band was not detected by a PRS-specific probe, suggesting transcript-directed synthesis of EPRS^{N1} (Figure 4A). IFN-γ, which induces EPRS phosphorylation and release from the MSC (Arif et al., 2009), did not alter the amount of either transcript. Cytosolic lysates were fractionated on a sucrose gradient, and total RNA from each fraction was subjected to northern analysis with an ERS-specific probe. Both full-length *EPRS* and *EPRS^{N1}* mRNAs were primarily found in the polysome fractions, indicating efficient translation (Figure 4B). Following G/I tailing (i.e., addition of polyG/I tails to total RNA) and RT-PCR, agarose gel electrophoresis detected polyadenylated products up to about 400 nt (Figure 4C, left). Sequencing of the 200 nt fraction revealed a cDNA identical to the N terminus of EPRS up to Tyr^{864}-encoding UAU, which is replaced by a UAA stop codon followed by a poly(A) tail without an intervening 3′ UTR (Figure 4C, right). *EPRS^{N1}* mRNA encodes ERS, WHEP R1, and the α helices of WHEP R2, but not the last 12 amino acids of R2. The region containing R1 and R2 binds GAIT-element RNA, whereas the linker region downstream of R2 contains IFN-γ-dependent phosphorylation sites required both for GAIT

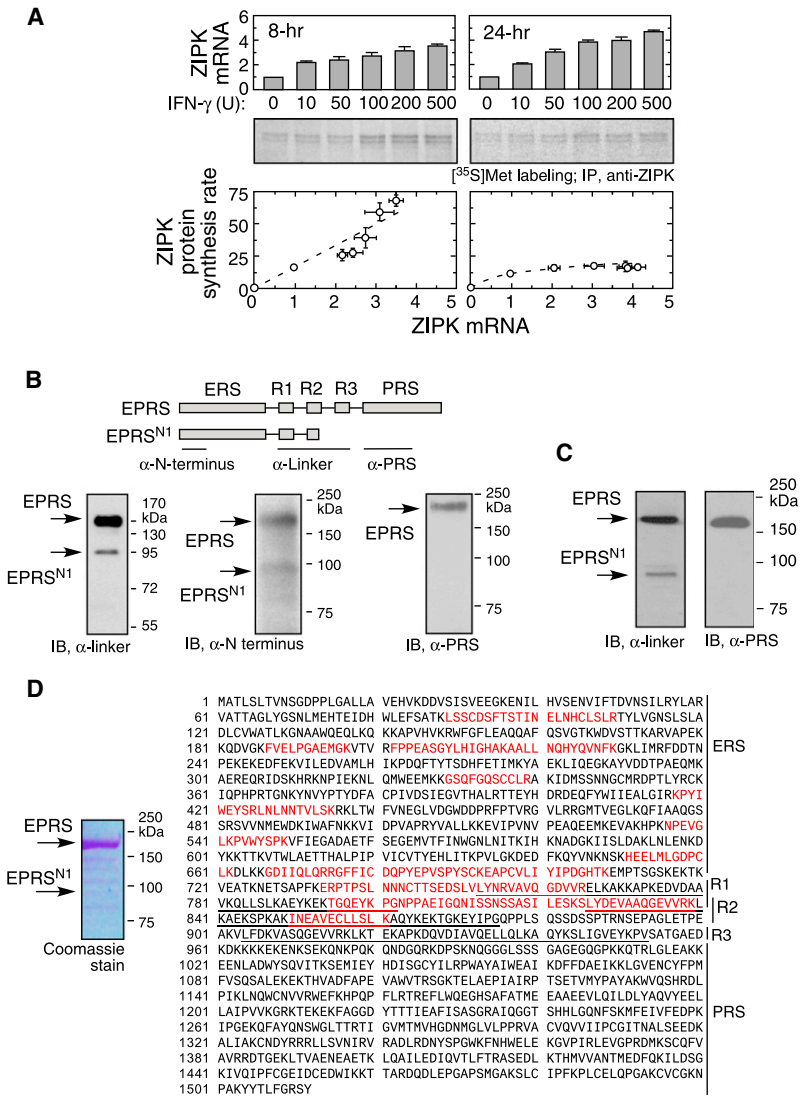

Figure 3. Monocytic Cells Contain a C-Terminal Truncated EPRS, EPRS^{N1}

(A) IFN-γ-stimulated monocytic cells maintain low-level synthesis of ZIPK. U937 cells were treated with IFN-γ as in Figure 1B. *ZIPK* mRNA was determined by qRT-PCR (top), and ZIPK synthesis determined by metabolic labeling with [^{35}S]Met followed by immunoprecipitation (IP) with anti-ZIPK antibody (middle). ZIPK protein synthesis as function of *ZIPK* mRNA is shown (mean ± SEM, n = 3) (bottom).

(B) Detection of EPRS^{N1} protein in U937 cells with domain-specific antibodies. Cytosolic lysates from U937 cells were subjected to immunoblot analysis with antibodies directed against EPRS linker domain, EPRS N-terminal peptide, and PRS.

(C) Presence of EPRS^{N1} in human PBM. Immunoblot analysis with antibodies directed against the EPRS linker and PRS domains.

(D) Mass spectrometric analysis indicates that EPRS^{N1} contains ERS, R1, and R2 domains but lacks R3 and PRS domains. EPRS^{N1} was isolated by immunoprecipitation with anti-EPRS linker antibody and SDS-PAGE and detected with Coomassie stain (left). Peptides detected by mass spectrometric analysis of a 95 kDa EPRS^{N1} band (red) and WHEP domains (underlined) are shown (right).

complex assembly and for GAIT function (Arif et al., 2009; Jia et al., 2008) (Figure 4D).

EPRS^{N1} Is Responsible for the Translational Trickle

To determine whether EPRS^{N1}, like EPRS, resides in the MSC and is released upon stimulation, U937 cells were transfected with c-Myc-tagged EPRS^{N1} and incubated with IFN-γ for up to 24 hr. The MSC was collected by immunoprecipitation with antibody against KRS, an MSC constituent. As shown before, full-length EPRS is present in the MSC and released upon IFN-γ treatment; however, EPRS^{N1} is not detected in the MSC (Figure 5A). The pre-GAIT and GAIT complexes were collected by immunoprecipitation with anti-NSAP1 antibody. As shown previously, IFN-γ induces translocation of full-length EPRS to the pre-GAIT complex (at 2 hr), where it is joined by other components to form the mature GAIT complex (at 14 hr), but neither complex contains EPRS^{N1}. The inability to bind NSAP1 confirms that EPRS^{N1} does not form the functional, heterotetrameric GAIT complex.

Based on the predicted binding activities, we considered that EPRS^{N1} might act as a dominant-negative inhibitor of the translational silencing activity directed by full-length EPRS. The interaction of EPRS^{N1} with GAIT-element RNA was determined by surface plasmon resonance (SPR) spectrometry. Recombinant EPRS^{N1} bound *Cp* GAIT-element RNA with a dissociation constant (K_D) of about 0.37 nM, whereas full-length EPRS bound with a K_D about 30-fold higher (Figure 5B). The high binding affinity of EPRS^{N1} was primarily due to a very low off-rate and suggests that EPRS^{N1} can effectively compete with GAIT complex for binding target mRNAs. EPRS^{N1} binding to inactive, mutant (U87C) *Cp* GAIT-element RNA was below the detection limit (not shown). To investigate binding in vivo, EPRS^{N1}-c-Myc was transfected into cells and immunoprecipitated with anti-c-Myc antibody, and bound RNA was detected by RT-PCR with mRNA-specific primers. Ectopically expressed EPRS^{N1} exhibited robust binding to *VEGF-A* but not *β-actin* mRNA, demonstrating specific interaction in cells as shown by RT-PCR (Figure 5C) and more quantitatively by qRT-PCR (Figure S2A). To determine its inhibitory activity, EPRS^{N1} was overexpressed in cells, and the interaction of the GAIT complex constituent L13a with *VEGF-A* mRNA was measured by RNA immunoprecipitation with anti-L13a antibody. Indeed, ectopic expression of EPRS^{N1} blocked L13a binding to *VEGF-A* mRNA, indicating effective competition, as shown by RT-PCR (Figure 5D) and qRT-PCR (Figure S2B).

To investigate the influence of EPRS^{N1} on GAIT target gene expression, we determined the effect of recombinant, His-tagged EPRS^{N1} on in vitro translation of a reporter RNA. VEGF-A GAIT-element-bearing firefly luciferase (FLuc) and renilla

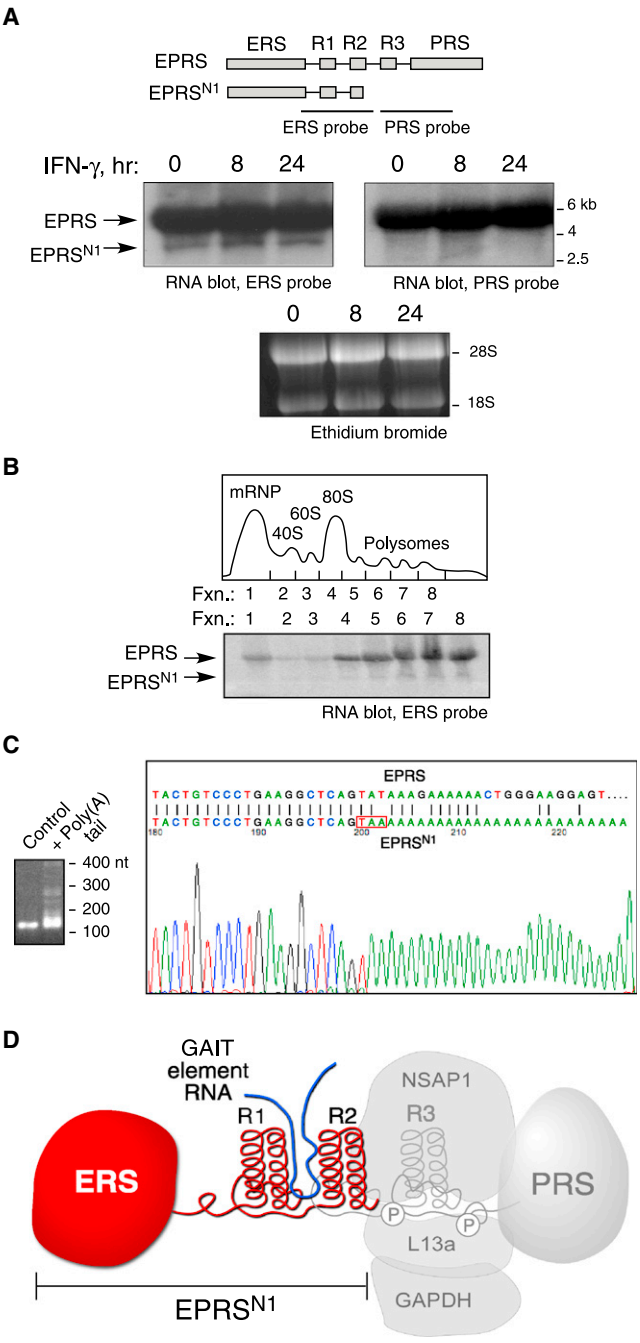

Figure 4. Monocytic Cells Express *EPRS^{N1}* mRNA

(A) *EPRS^{N1}* mRNA is expressed constitutively. Total RNA from U937 cells treated with IFN-γ was subjected to RNA blot analysis using ERS- and PRS-specific probes.

(B) *EPRS^{N1}* mRNA is translatable. U937 cell lysates were fractionated on a sucrose gradient, and extracted RNA in each fraction was subjected to RNA blot analysis with ERS-specific probe.

(C) Nucleotide sequence of *EPRS^{N1}* mRNA. G/I stretches were added to poly(A)-tailed mRNA, RT-PCR was done using oligo-C and gene-specific upstream primers, and the amplified fragment was cloned into T-vector and sequenced.

(D) Schematic of EPRS^{N1} structure in context of full-length EPRS, its phosphorylation sites, and its binding partners.

luciferase (RLuc) control RNAs were cotranslated in rabbit reticulocyte lysate (RRL) in the presence of cytosolic lysate from IFN-γ-treated cells. As shown previously, 24 hr lysate specifically inhibited translation of GAIT-element-bearing mRNA (Jia et al., 2008); however, EPRS^{N1} almost completely restored expression (Figure 5E). To determine the mechanism of translational inhibition, lysates from c-Myc-tagged EPRS^{N1}-transfected, IFN-γ-treated cells were fractionated on a sucrose gradient, and *VEGF-A* mRNA was determined by RT-PCR. A near-complete shift of *VEGF-A* mRNA from a translationally silent mRNP pool to the translationally active polysome fractions indicated that EPRS^{N1} prevents GAIT complex-mediated inhibition of target mRNA translation (Figure 5F). To show that EPRS^{N1} affects endogenous gene expression, transfected U937 cells were treated with IFN-γ, and VEGF-A and Cp expression measured by immunoblot. Overexpression of EPRS^{N1} markedly increased in vivo expression of GAIT target proteins after 24 hr IFN-γ treatment compared to transfection controls (Figure 5G, left). *VEGF-A* mRNA expression was not significantly increased by ectopic expression of EPRS^{N1} (Figure 5G, right). The nearly 2-fold increase in *Cp* mRNA is expected to have a small effect on protein expression, as shown by an undetectable increase in protein following 4- to 8-fold increases in *VEGF-A* or *ZIPK* mRNA, respectively (Figures 1B and 3A), and certainly cannot account for the observed 5-fold increase in Cp protein expression. These experiments demonstrate that EPRS^{N1}, by high-affinity binding to GAIT target mRNAs, protects a small amount of mRNA from GAIT complex-mediated translational silencing, thereby maintaining low-level expression of target protein despite high-level induction of mRNA. Thus, EPRS^{N1} is the GEIF predicted by the modeling studies described above.

EPRS^{N1} Is Generated by Polyadenylation-Mediated Tyr-to-Stop Codon Conversion

Analysis of human genome sequence databases did not reveal a duplicated *EPRS* gene. Moreover, the substitution of a Tyr-encoding UAU codon in *EPRS* mRNA with a UAA stop codon followed by poly(A) in *EPRS^{N1}* mRNA was not consistent with an alternative splicing mechanism. We considered the possibility that *EPRS^{N1}* mRNA might be generated by an alternative polyadenylation (APA) event within the *EPRS* mRNA coding region that recodes a Tyr codon to a stop. Polyadenylation generally utilizes a $^{C}/_{U}$A cleavage site, an upstream hexanucleotide element (AAUAAA) or its variant (AUUAAA), and a downstream U- or GU-rich element, although these requirements are not absolute (Birnstiel et al., 1985). Inspection of *EPRS* mRNA sequence near the *EPRS^{N1}* 3′ terminus revealed a UA cleavage site within the terminal Tyr codon, a consensus upstream hexanucleotide element at −40 (relative to the cleavage site), and a downstream U-rich element at +117 (Figure 6A). To provide evidence for polyadenylation-mediated Tyr-to-stop codon conversion (PAY*) and verify the *cis*-acting signal elements, we subjected a [^{32}P]UTP-labeled polyadenylation cassette to an in vitro cleavage assay (Ahmed et al., 1991; Bar-Shira et al., 1991; Hans and Alwine, 2000; Wu and Alwine, 2004). The 240 nt APA cassette RNA, containing the cleavage site and putative upstream and downstream elements, was cleaved into a 109 nt 5′ RNA product by nuclear extract from U937 cells (Figure 6B).

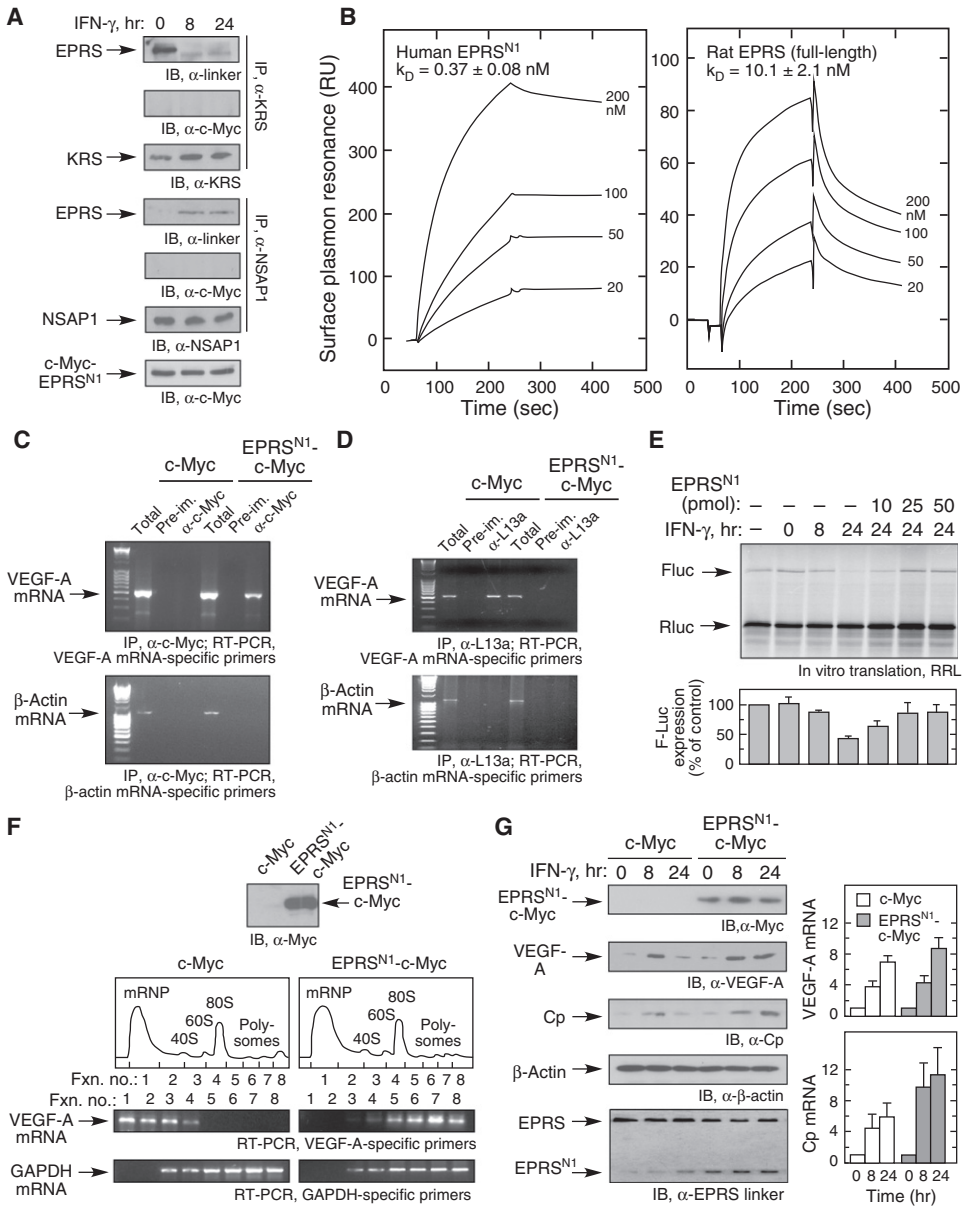

Figure 5. EPRS^{N1} Binding to GAIT-Element RNA Blocks Translational Repression

(A) EPRS^{N1} exists as a free protein outside the MSC or GAIT complex. U937 cells were transfected with pcDNA3.1-EPRS^{N1}-Myc plasmid and treated with IFN-γ for up to 24 hr. Cell lysates were immunoprecipitated with anti-KRS and anti-NSAP1 antibodies, then subjected to immunoblot with anti-EPRS linker and anti-Myc tag antibodies.

(B) High-affinity binding of EPRS^{N1} to GAIT RNA element. Biotinylated, 29 nt Cp GAIT-element RNA was immobilized on a streptavidin sensor chip. Binding of human EPRS^{N1} (left) and full-length rat EPRS (right) was determined by SPR and expressed as RU.

(C) EPRS^{N1} interacts with *VEGF-A* mRNA in vivo. U937 cells were transfected with pcDNA3.1-EPRS^{N1}-Myc or Myc vector control, and lysates immunoprecipitated (IP) with anti-Myc antibody. Extracted RNA was subjected to RT-PCR using primers specific for *VEGF-A* or *β-actin* mRNA.

(D) EPRS^{N1} inhibits GAIT complex binding to *VEGF-A* mRNA. U937 cells were transfected with pcDNA3.1-EPRS^{N1}-Myc or vector control, and GAIT complex in lysates was immunoprecipitated with anti-L13a antibody. Extracted RNA was subjected to RT-PCR as in (C).

(E) Recombinant EPRS^{N1} restores in vitro translation of the GAIT-element-bearing reporter. In vitro translation of the FLuc reporter bearing the *VEGF-A* GAIT element (and RLuc control RNA) was determined in a rabbit reticulocyte lysate (RRL) in the presence of [^{35}S]Met, cytosolic extracts from IFN-γ-treated U937 cells, and recombinant EPRS^{N1}. FLuc expression was quantitated by densitometry, normalized by RLuc expression, and reported as mean ± standard deviation (SD) (n = 3).

(F) EPRS^{N1} restores translation of endogenous GAIT-element-bearing mRNAs. Lysates from U937 cells transfected with pcDNA3.1-EPRS^{N1}-Myc were fractionated on a sucrose gradient, and total RNA subjected to RT-PCR with VEGF-A- and GAPDH-specific primers.

(G) EPRS^{N1} restores expression of GAIT-element-bearing mRNAs. U937 cells were transfected with pcDNA3.1-EPRS^{N1}-Myc and treated with IFN-γ for up to 24 hr. Cell lysates were subjected to immunoblot (left) and qRT-PCR (right) analyses as shown. The relative *VEGF-A* and *Cp* mRNA levels were reported as mean ± SEM (n = 3).

See also Figure S2.

Mutation of the UA cleavage site or the upstream or downstream elements prevented cleavage, as did immunodepletion of cleavage and polyadenylation stimulation factor-100 (CPSF100). In vitro polyadenylation of the precleaved RNA cassette likewise was consistent with the in vitro cleavage results (Figure 6C).

To investigate the role of the PAY* mechanism in vivo, a reporter plasmid was generated by subcloning the polyadenylation cassette downstream of the RLuc coding region to replace the SV40 late cassette in the pRL-SV40 plasmid. This assay is based on the requirement for transcript polyadenylation for efficient translation (McMahon et al., 2006). The reporter was cotransfected with a plasmid encoding FLuc as a control for transfection efficiency. The wild-type cassette was expressed much more efficiently than either the upstream or downstream mutants, consistent with in-CDS (in-coding sequence) APA in cells (Figure 6D). To verify the activity of endogenous EPRS^{N1}, U937 cells (Figure 6E) and human PBM (Figure S3A) were transfected with antisense morpholino oligomer targeting the alternative cleavage site. The morpholino reduced EPRS^{N1} expression by about 75% and concomitantly reduced the VEGF-A trickle level by about the same amount (Figure 6E), consistent with the simulation results (Figure 2C, right, 0.25× GEIF). These data support the PAY* mechanism and verify that EPRS^{N1} is responsible for maintaining the translational trickle of VEGF-A expression.

Transcriptome Expansion by the PAY* Mechanism

We used a bioinformatic approach to globally seek candidate mRNAs generated by PAY*. The human expressed sequence tag (EST) and mRNA databases were queried with two criteria: (1) coding RNA has a poly(A) tail immediately downstream of the first UAA stop codon, and (2) the UAA stop codon replaces a Tyr-encoding UAU or UAC in a larger transcript that extends 3′ beyond the truncated mRNA (Figures S3B and S3C). Seven candidate transcripts fulfilling both criteria were identified; among them only ribonucleotide reductase M1 (*RRM1*), an important cancer marker gene, exhibited a perfect consensus upstream element (at position −18) within the same exon as the cleavage site (Figure S3D). Two-round nested RT-PCR of U937 cell RNA revealed the truncated form of *RRM1* (*RRM1*^{N1}) (Figure 6F). We cannot exclude the possibility that other candidate truncated mRNAs might be found in other cell types or under other conditions. RNA blot analysis with 5′- and 3′-specific RRM1 probes verified the presence of the C-terminal truncated form (Figure 6G). Sucrose gradient fractionation of cell lysate followed by northern analysis with an N terminus-specific RRM1 probe confirmed low-level expression of *RRM1*^{N1} (compared to the full-length mRNA) and also showed strong association with polysomes indicative of active translation (Figure 6H). Immunoblot analysis of cell lysates with antibodies generated against the N and C termini of RRM1 confirmed the presence of both full-length RRM1 and RRM1^{N1} in human PBM (data not shown) and U937 cells (Figure 6I).

DISCUSSION

Dynamic modeling of the GAIT system, coupled with experimental validation, revealed two EPRS isoforms, a full-length form residing in the MSC and GAIT complex and a truncated free form, ERPS^{N1}. ERPS^{N1} performs a function closely related to the noncanonical function of the parental form, namely, acting as a dominant-negative inhibitor that prevents complete translational silencing of target transcripts by the GAIT complex. Thus EPRS joins a select group of AARS that exhibit a noncanonical activity requiring a truncation event that reveals a cryptic stimulatory domain or removes an inhibitory peptide. For example, proteolytic removal of the EMAPII domain from YRS unmasks a tripeptide motif that confers proangiogenic activity (Wakasugi and Schimmel, 1999). Likewise, deletion of a WHEP domain from WRS by proteolysis or alternative splicing generates an antiangiogenic protein (Wakasugi et al., 2002). RRS exhibits two isoforms produced by alternative translation initiation from a single mRNA; the larger isoform resides in the MSC, whereas the smaller isoform is free (Kyriacou and Deutscher, 2008).

ERPS^{N1} is constitutively generated by an unanticipated PAY* mechanism within the coding region of *EPRS*. APA generally occurs in noncoding regions of mRNAs, most often distal to the stop codon generating mRNAs with a shorter 3′ UTR, thereby eliminating sites of posttranscriptional regulation (Danckwardt et al., 2008; Edwalds-Gilbert et al., 1997; Licatalosi and Darnell, 2010; Millevoi and Vagner, 2010). Less frequently, APA occurs distal to a stop codon in a cryptic intron to generate a truncated mRNA and protein, with an appended C-terminal sequence encoded by the intron (Figure S4A) (Di Giammartino et al., 2011). In mitochondria, a poly(A) tail can be appended to a 3′-terminal U or UA to generate a UAA stop codon; however, unlike PAY*, this mechanism does not generate an alternative mRNA or protein but instead has evolved to maintain the small size of the mitochondrial genome by eliminating the 3′ UTR (Figure S4A) (Anderson et al., 1981). APA within the coding sequence of several genes generates truncated transcripts lacking a stop codon and subjected to exosome-mediated, nonstop mRNA decay (Frischmeyer et al., 2002; van Hoof et al., 2002). Here, we show an example of generation of a stable truncated mRNA by APA within a coding region driven by recoding of an in-frame Tyr codon to a stop codon, generating a 3′-truncated, 3′ UTR-less mRNA and a C-terminal truncated protein (Figure 7A). The absence of any 3′ UTR in transcripts generated by the PAY* mechanism depletes posttranscriptional regulatory elements, including protein- and microRNA-binding sites (Mayr and Bartel, 2009). The relatively inefficient generation of EPRS^{N1} mRNA and protein might be due to suboptimal location of the polyadenylation elements. About 0.7% of human mRNAs are predicted to contain APA signal elements within the CDS (Frischmeyer et al., 2002). In addition to myeloid cells, EPRS^{N1} is constitutively expressed by multiple types of human cells, including umbilical vein and microvascular endothelial cells, hepatoma-derived HepG2 cells, embryonic kidney HEK293T cells, and cervical carcinoma HeLa cells (Figure S4B). Inspection of *EPRS* mRNA sequences from several species shows that the required elements are conserved in primates, e.g., gorilla, chimpanzee, and macaque, but not in several other mammals, e.g., dog, cow, rabbit, pig, and mouse (Figure S4C). Northern analysis confirmed the absence of a truncated *EPRS* mRNA in mouse RAW 264.7 cells (Figure S4D). Thus, PAY*-mediated generation

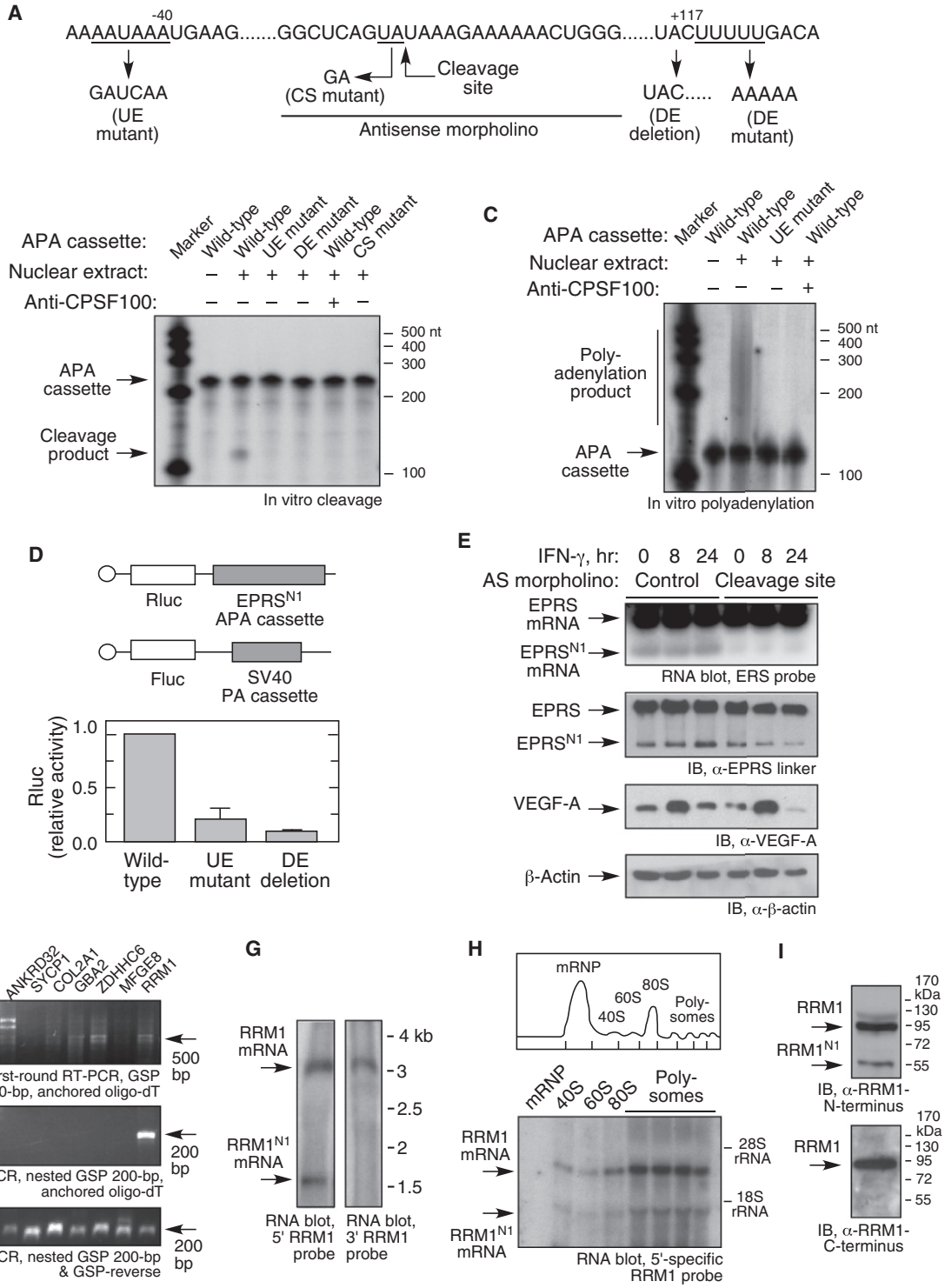

Figure 6. *EPRS*^{N1} mRNA Is Generated from *EPRS* mRNA by the PAY* Mechanism

(A) *EPRS* mRNA cassette containing upstream (UE) and downstream (DE) APA signal elements and cleavage site (CS).

(B) In vitro cleavage assay for analysis of polyadenylation signal elements. [^{32}P]UTP internal-labeled RNA cassettes from −109 to +131 relative to the cleavage site, containing the putative APA elements and mutants, were generated by in vitro transcription and subjected to an in vitro cleavage assay in presence of nuclear extracts from U937 cells.

(C) In vitro polyadenylation of *EPRS*^{N1} precleaved RNA. A precleaved, [^{32}P]UTP internal-labeled, 109 nt RNA was generated from the polyadenylation cassette by in vitro transcription and used in an in vitro polyadenylation assay in which substrate RNA is mixed with nuclear extract and ATP.

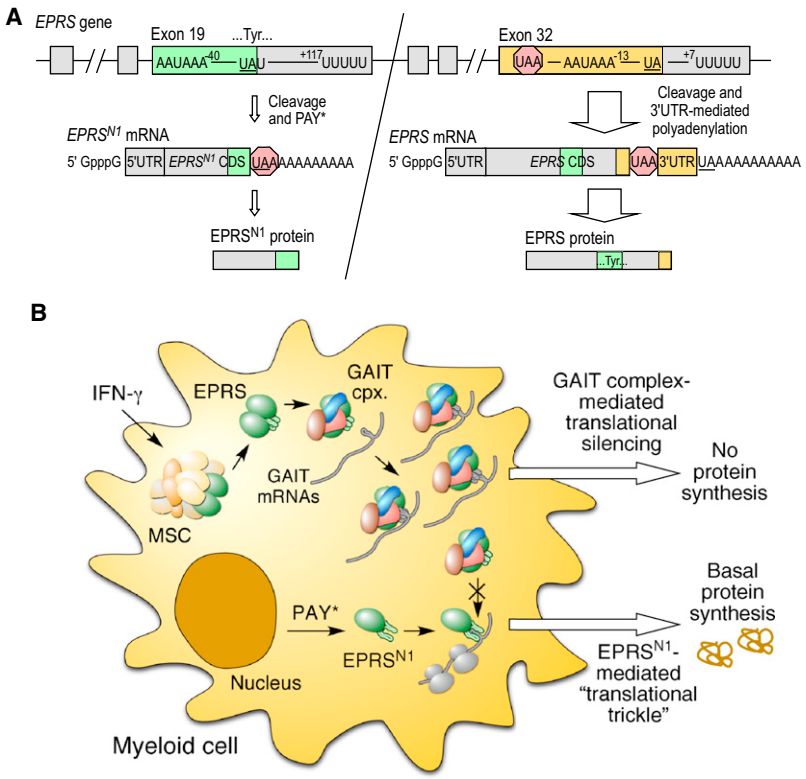

Figure 7. Schematics of EPRS^{N1} Generation by PAY* and Function in Gene Expression

(A) Pathways of EPRS^{N1} expression by PAY* (left) and EPRS expression by 3′ UTR-based polyadenylation (right). Exon segments of *EPRS^{N1}* (green) and *EPRS* (brown) upstream of the cleavage sites (underlined) are indicated.

(B) EPRS^{N1} function in maintaining a translational trickle of inflammatory gene expression in myeloid cells.

See also Figure S4.

of *EPRS^{N1}* might be a recently evolved, species-selective mechanism of gene regulation.

Our results reveal an atypical negative-regulatory mechanism in which constitutive, low-level expression of a high-affinity competitor such as EPRS^{N1} shields a small, constant amount of GAIT target transcripts from translational repression. The GAIT complex can be considered as a closed gate that blocks translation of select transcripts following proinflammatory stimulation by IFN-γ, whereas, EPRS^{N1} can be considered as a "doorstop" that prevents complete closure of the gate, permitting a translational trickle of target expression (Figure 7B). The GAIT target VEGF-A is a potent macrophage-derived angiogenic factor co-opted by tumors to induce blood vessel development and facilitate tumor growth and metastasis (Tammela et al., 2005). Anti-VEGF therapy successfully limits colorectal and renal cell carcinoma (Kamba and McDonald, 2007); however, adverse effects of these therapies, including blood vessel regression, suggests that VEGF-A is essential for maintenance of healthy vessels as well as for development. Moreover, recent studies show that conditional deletion of macrophage-derived VEGF-A results in accelerated tumor growth (Stockmann et al., 2008). We suggest that a major function of EPRS^{N1} is to maintain VEGF-A, and other proinflammatory proteins, at basal levels required for tissue health and organismal advantage. The possible function of RRM1^{N1} is less clear. RRM1 is the catalyst of deoxyribonuclotide synthesis during DNA synthesis and cell division and is the molecular target of gemcitabine for treatment of cancer (Jordheim et al., 2011). RRM1^{N1} contains the effector binding site and partial catalytic active site but lacks the C terminus required for high-affinity binding to its regulated partner RRM2, which conceivably could reduce RRM1 activity or contribute to gemcitabine resistance. The discovery of multiple potential PAY* targets, and the validation of *RRM1*, indicates that PAY* might be a fundamental mechanism of transcriptome and proteome expansion.

Organisms have evolved multiple mechanisms to compel low-level or basal amounts of important molecules under conditions in which there is both inductive synthetic pressure as well as negative regulation to prevent excessive expression. The most common regulatory mechanisms involve negative-feedback loops. For example, the inducible c-*fos* transcription factor binds and represses its own promoter, thereby maintaining intermediate levels of the transcription factor and its inducible targets (Sassone-Corsi et al., 1988). More complex systems involving multiple feedback loops can also maintain gene expression within defined limits. As one example, delayed proteasomal degradation of the bHLH transcription suppressor Hes1 results

(D) In vivo polyadenylation of *EPRS^{N1}* APA cassette. U937 cells were transfected with RLuc reporter plasmids containing wild-type and mutant *EPRS^{N1}* APA cassettes and FLuc reporter plasmid as transfection efficiency control. After 24 hr, luciferase activity of cell extracts was determined.

(E) Reduction of EPRS^{N1} expression diminishes the translational trickle of VEGF-A. U937 cells transfected with an antisense morpholino oligomer targeting the cleavage site were treated with IFN-γ. *EPRS* and *EPRS^{N1}* mRNA were determined by RNA blot with an ERS-specific probe, and protein by immunoblot with anti-linker antibody. VEGF-A and β-actin in cell lysates were determined by immunoblot.

(F) Truncated form of *RRM1* mRNA is produced by an in-CDS alternative polyadenylation mechanism. Total RNA from U937 cells was subjected to two-round nested RT-PCR using gene-specific primers (GSP). Full-length mRNA expression was determined by RT-PCR.

(G) Detection of *RRM1^{N1}* mRNA. Total RNA from U937 cells was subjected to RNA blot analysis using 5′- and 3′-specific RRM1 probes.

(H) Truncated mRNA of *RRM1* is actively translatable. U937 cell lysates were fractionated by polysome profiling. The total RNA from various fractions was extracted and subjected to northern blot analysis with RRM1 5′-specific probe.

(I) Detection of RRM1^{N1} protein. Western blot was performed with N terminus- and C terminus-specific antibody against RRM1.

See also Figure S3.

in oscillatory expression of the factor. The oscillation (and frequency) is established by a pair of temporally displaced regulatory loops, a feature common to circadian and other oscillatory circuits (Hirata et al., 2002). MicroRNAs exert posttranscriptional control of gene expression by diverse mechanisms (Leung and Sharp, 2010). Every microRNA targets multiple mRNAs, and most mRNAs bind multiple regulatory miRNAs. The net output is determined by the relative cellular concentration of the miRNA ensemble and their target mRNAs. Although individual microRNAs generally inhibit protein production by small amounts, usually much less than 50%, the sum of targeting microRNAs can completely switch off gene expression when and where necessary. In other cases, microRNAs perform subtle "tuning" functions (Bartel, 2009). For example, atrophin is repressed by miR-8 in *Drosophila* but not to the low level detrimental to cell viability (Karres et al., 2007). The mechanism by which appropriate microRNA-to-target stoichiometry is controlled to maintain optimal protein output is not well understood, but negative-feedback loops might be important. For example, stress-inducible, proinflammatory activation of the NF-κB transcription in macrophages induces a family of microRNAs that target and repress proinflammatory signaling molecules, including NF-κB (Leung and Sharp, 2010). The timescale of induction, maturation, and accumulation of these microRNAs is about 24 hr. This delayed temporal response is suggested to permit a vigorous inflammatory defense against pathogens while constraining the response duration to minimize host injury. To our knowledge, there are not any reports of systems comparable to the GAIT system in which endogenous, transcript-selective RNA-binding proteins act as dominant-negative repressors. In the *Pseudomonas* RsmA-RsmZ regulatory system, the primary inhibitor, RsmA, binds the 5′ UTR of target mRNAs and inhibits their translation (Heeb et al., 2002). The secondary regulator, RsmZ, is a small RNA that acts as an RNA decoy, binding RsmA and reducing its translational repression activity. This system is different from the EPRS/EPRS^{N1} system in which the secondary regulator, i.e., EPRS^{N1}, binds target mRNAs, not the GAIT complex primary inhibitor. Our modeling studies show that modulation of RsmA by RsmZ will indeed relieve translational repression but will not generate the nonlinear translational trickle characteristic of our newly described mechanism (Figures S1A–S1D).

We propose that the GAIT complex exerts a protective function as a delayed translational repressor of inflammatory gene expression, whereas EPRS^{N1} prevents repression below basal amounts. Thus, regulation is broadly exerted on a posttranscriptional regulon united by a common structural RNA element. Importantly, this regulatory mechanism is superimposed on the identical regulon controlled by the GAIT complex. We envision the presence of similar regulatory systems that generate translational trickles of distinct mRNA families. The system requirements include low-level expression of a fragment of an RNA-binding protein that binds RNA elements in a posttranscriptional mRNA regulon. The fragment is likely to bind the element with an affinity substantially higher than the parental RNA-binding protein. Also, the fragment must be defective with respect to translational silencing activity, possibly by preventing holo-complex formation or by direct inactivation of the inhibitory function. Our results have not yet revealed regulation of EPRS^{N1} production; however, this is not a necessary system attribute, and indeed the level of the trickle might be regulated in the GAIT system (e.g., by condition-dependent regulation of PAY* activity) and in other systems. The GAIT/EPRS^{N1} system is characterized by constitutive, low-level expression of EPRS^{N1}, established by an intrinsically inefficient PAY* mechanism, and the absence of any 3′ UTR in *EPRS^{N1}* contributes to the lack of regulation. The EPRS^{N1}-driven regulatory system represents an unusual "bottom-up" mechanism. Instead of the usual mechanism in which low-level amounts of protein products are maintained by restricting the inhibitory activity, EPRS^{N1} exerts a stimulatory activity that is totally independent of other stimulatory or inhibitory activities, including feedback inhibition. In total, these attributes result in a regulatory mechanism that ensures a constant, low-level trickle of target protein expression even under strong negative pressure.

EXPERIMENTAL PROCEDURES

Modeling Procedures

Development and application of dynamic models to simulate the GAIT system are described in the Extended Experimental Procedures.

Cell Culture

Human U937 monocytic cells (ATCC, Rockville, MD, USA) and primary human PBM (from healthy clinical donors) were cultured in RPMI 1640 medium containing 10% fetal bovine serum (FBS). For preparation of cytosolic extracts, the cells were incubated for 1 hr in medium containing 0.5% FBS and then incubated with IFN-γ for an additional 8 or 24 hr.

Plasmids, Site-Directed Mutagenesis, and Recombinant Protein Expression

EPRS^{N1} (Met1 to Gln863) was cloned into a pET-28 expression vector between SacI and SalI restriction sites and expressed as described (Jia et al., 2008). pcDNA3.1-EPRS^{N1}-c-Myc was generated with pET28-EPRS^{N1} as template and cloned between NotI and XbaI restriction sites. The DNA template for in vitro transcription of *EPRS^{N1}* polyadenylation cassette RNA was cloned into PSP64 vector (PSP64-PAC) between SalI and EcoRI restriction sites. Specific mutations for *EPRS^{N1}* polyadenylation cassette RNA were introduced into PSP64-PAC by PCR-based mutagenesis. The reporter plasmids were constructed by subcloning polyadenylation cassettes into pRL-SV40 reporter plasmid between XbaI and BamHI sites. The SV40 polyadenylation cassette was replaced by *EPRS^{N1}* polyadenylation cassette.

Immunoprecipitation and Immunodepletion

For immunoprecipitation, cell lysates prepared in phospho-safe extraction buffer were precleared with protein A/G-agarose beads. After centrifugation, the supernatants were combined with protein A/G beads and antibody and incubated with rotation at 4°C for 4 hr. The beads were washed with cold cell lysis buffer. Protein gel loading dye was added and the samples boiled before gel-loading. For immunodepletion, nuclear extracts from U937 cells were incubated with rabbit anti-CPSF100 antibody coupled to protein A/G-agarose beads in extraction buffer. The beads were pelleted, the supernatants subjected to two additional rounds of depletion, and immunodepletion established by immunoblot with mouse anti-CPSF100 antibody.

RNA Blot Analysis

For RNA blot analysis, total RNA was extracted from 10^8 U937 cells using Trizol reagent. RNA (20 μg) was fractionated on 1% agarose-formaldehyde gel and transferred to Zeta-Probe GT membrane. The blot was hybridized with random primer-labeled cDNA probes, and the signal scanned and quantified by Phosphoimager. qRT-PCR determinations of *VEGF-A*, *Cp*, and *GAPDH* mRNA were done with the Taqman Gene Expression Assays for various targets and the StepOnePlus Real-Time PCR System.

RIP-RT-PCR

Cell lysates were immunoprecipitated with mouse anti-c-Myc antibody or preimmune IgG as above. Total and immunoprecipitated RNA were extracted separately with Trizol reagent, subjected to RT-PCR with Taq DNA polymerase, and visualized by 1.5% agarose gel.

Mass Spectrometry

Proteins immunoprecipitated by anti-EPRS linker antibody from U937 cell lysates were resolved by 4%–20% SDS-PAGE gel. The 95 kDa, Coomassie-stained band was in-gel digested with trypsin and analyzed by capillary liquid chromatography tandem mass spectrometry (LC-MS/MS) analysis. CID spectra were queried against the human reference sequence database using Mascot software, and matching spectra verified manually and with the Sequest and Blast as needed.

G/I Tailing and cDNA Cloning

Total RNA from U937 cells was extracted with Trizol reageat and subjected to G/I tailing following the protocol from the Poly(A) Tail-Length Assay Kit. Poly(G/I)-tailed RNA product was subjected to RT-PCR, and the reaction product loaded onto a 2.5% agarose TBE gel. The band with lowest molecular weight was removed, purified, and ligated into pGEM-T vector for DNA sequencing.

Polysome Profiling

Cells were preincubated with cycloheximide (CHX, 100 μg/ml) for 15 min and washed twice with CHX-containing cold PBS. Cells were suspended in TMK lysis buffer, the lysates were centrifuged, and the supernatant collected. Sucrose gradient solutions (10% and 50%) containing RNase inhibitor and CHX were freshly prepared. The cytosolic lysates were loaded on the sucrose gradient, centrifuged at 29,000 rpm for 4 hr, and subjected to gradient fractionation.

In Vitro Translation

Capped, poly(A)-tailed template mRNAs were prepared with mMESSAGE mMACHINE SP6 and T7 kits. FLuc-VEGF-A GAIT element-poly(A) and RLuc reporter RNAs were incubated with U937 cytosolic extract in the presence of rabbit reticulocyte lysate and [^{35}S]methionine for 90 min at 30°C, resolved by 10% SDS-PAGE gel, and visualized by Phosphorimager.

RNA-Protein Interaction by SPR

Protein binding to *Cp* GAIT-element RNA was determined by SPR in a Biacore 3000 system (Jia et al., 2008). Biotinylated, wild-type, and mutant GAIT-element RNA (U87C) were separately immobilized on a streptavidin sensor chip in HBS-P buffer. The analyte flow rate was 5 μl/min in the same buffer containing 5 mM $MgCl_2$. Dissociation constants were calculated for a range of protein concentrations using Biaevaluation software.

In Vitro Cleavage and Polyadenylation Assays

The polyadenylation cassette RNA was transcribed using a MAXIscript SP6 in vitro transcription kit. Transcribed RNA was dephosphorylated with calf intestinal phosphatase (CIP) at 37°C for 30 min, and CIP was removed by phenol/chloroform extraction. The RNA product was 5′-end labeled with ^{32}P-γ-ATP catalyzed by polynucleotide kinase at 37°C for 1 hr and purified using a Micro Bio-Spin 30 chromatography column. To measure cleavage reaction, the ^{32}P-labeled polyadenylation cassette RNA was incubated with U937 nuclear extract (50%, v/v), KCl (50 mM), $MgCl_2$ (1 mM), EDTA (0.1 mM), glycerol (10%), DTT (0.2 mM), creatine phosphate (20 mM), and polyvinyl alcohol (2%). For in vitro polyadenylation assay, 1 mM ATP was added to the same reaction solution in the presence of precleaved polyadenylation cassette RNA.

Cell Transfection and Dual Luciferase Reporter Assay

U937 cells were transiently cotransfected with 0.5 μg pRL-SV40 plasmid (containing polyadenylation cassette) and 1 μg pCD-FLuc (for normalization of transfection efficiency) using a human monocyte nucleofector kit. After 24 hr, transfected cells were lysed, and luciferase activity of the lysates was measured with the Dual Luciferase Reporter assay system. To knock down endogenous EPRS^{N1}, U937 cells were transfected with morpholino antisense oligomers or a control morpholino oligomer with a human monocyte nucleofector kit.

Global Detection of Candidate PAY* mRNAs

We examined a collection of 19,629 human reference genes (RefGene) in the University of California at Santa Cruz (UCSC) Genome Browser, including genomic information on start and stop codon positions and 3′ and 5′ splice sites. 3′ UTR-less PAY* transcripts were sought using sequence and genomic alignment information of human ESTs and mRNAs available in the UCSC Genome Browser. Sequences with tracts (defined as 10 or more contiguous nt) of poly(A) in the 3′ end or poly(T) in the 5′ end (for reverse-complemented ESTs or mRNAs) were identified as poly(A) ESTs or mRNAs. The first A or T in the poly(A) or poly(T) tract was considered to be the transcript poly(A) site and is required to be upstream or downstream 5 nt from the nearest alignment site on the genome. The poly(A) tail of ESTs or mRNAs was required to be absent (less than 18 A's within 20 bp downstream or upstream of the poly[A] site) in the corresponding genome region to eliminate internal priming sites. When a poly(A)-containing EST or mRNA shared all internal splice sites with a RefGene, that RefGene was assigned as reference, and the start codon position was inferred by the ORF of its RefGene. If the first stop codon coincided with the start of the poly(A) tail, then the poly(A) sequence was considered as a 3′ UTR-less, in-CDS EST or mRNA. From this group, PAY* candidates were selected by replacement of TAT or TAC Tyr codons with a TAA stop codon in 3′ UTR-less in-CDS ESTs or mRNAs.

Nested RT-PCR for Detecting Candidate mRNAs Generated by PAY*

Total RNA was extracted from U937 cells and subjected to reverse transcription using oligo-dT primer. Two-round nested PCR was performed with the cDNA as template.

SUPPLEMENTAL INFORMATION

Supplemental Information includes Extended Experimental Procedures, four figures, and two tables and can be found with this article online at doi:10.1016/j.cell.2012.02.018.

ACKNOWLEDGMENTS

We are grateful to Richard Padgett for helpful discussions and David Dignam for the gift of anti-PRS antibody. This work was supported in part by National Institutes of Health grants P01 HL029582, P01 HL076491, R01 GM086430, and R01 DK083359 to P.L.F. P.Y. was supported by a Postdoctoral Fellowship from the American Heart Association, Great Rivers Affiliate, and A.A. by National Center Scientist Development Grant 10SDG3930003 from the American Heart Association.

Received: June 27, 2011
Revised: October 29, 2011
Accepted: February 9, 2012
Published online: March 1, 2012

REFERENCES

Ahmed, Y.F., Gilmartin, G.M., Hanly, S.M., Nevins, J.R., and Greene, W.C. (1991). The HTLV-I Rex response element mediates a novel form of mRNA polyadenylation. Cell *64*, 727–737.

Anderson, S., Bankier, A.T., Barrell, B.G., de Bruijn, M.H., Coulson, A.R., Drouin, J., Eperon, I.C., Nierlich, D.P., Roe, B.A., Sanger, F., et al. (1981). Sequence and organization of the human mitochondrial genome. Nature *290*, 457–465.

Arif, A., Jia, J., Moodt, R.A., DiCorleto, P.E., and Fox, P.L. (2011). Phosphorylation of glutamyl-prolyl tRNA synthetase by cyclin-dependent kinase 5 dictates transcript-selective translational control. Proc. Natl. Acad. Sci. USA *108*, 1415–1420.

Arif, A., Jia, J., Mukhopadhyay, R., Willard, B., Kinter, M., and Fox, P.L. (2009). Two-site phosphorylation of EPRS coordinates multimodal regulation of noncanonical translational control activity. Mol. Cell *35*, 164–180.

Bar-Shira, A., Panet, A., and Honigman, A. (1991). An RNA secondary structure juxtaposes two remote genetic signals for human T-cell leukemia virus type I RNA 3′-end processing. J. Virol. *65*, 5165–5173.

Bartel, D.P. (2009). MicroRNAs: target recognition and regulatory functions. Cell *136*, 215–233.

Birnstiel, M.L., Busslinger, M., and Strub, K. (1985). Transcription termination and 3′ processing: the end is in site!. Cell *41*, 349–359.

Cahuzac, B., Berthonneau, E., Birlirakis, N., Guittet, E., and Mirande, M. (2000). A recurrent RNA-binding domain is appended to eukaryotic aminoacyl-tRNA synthetases. EMBO J. *19*, 445–452.

Danckwardt, S., Hentze, M.W., and Kulozik, A.E. (2008). 3′ end mRNA processing: molecular mechanisms and implications for health and disease. EMBO J. *27*, 482–498.

Di Giammartino, D.C., Nishida, K., and Manley, J.L. (2011). Mechanisms and consequences of alternative polyadenylation. Mol. Cell *43*, 853–866.

Edwalds-Gilbert, G., Veraldi, K.L., and Milcarek, C. (1997). Alternative poly(A) site selection in complex transcription units: means to an end? Nucleic Acids Res. *25*, 2547–2561.

Frischmeyer, P.A., van Hoof, A., O'Donnell, K., Guerrerio, A.L., Parker, R., and Dietz, H.C. (2002). An mRNA surveillance mechanism that eliminates transcripts lacking termination codons. Science *295*, 2258–2261.

Guo, M., Yang, X.L., and Schimmel, P. (2010). New functions of aminoacyl-tRNA synthetases beyond translation. Nat. Rev. Mol. Cell Biol. *11*, 668–674.

Hans, H., and Alwine, J.C. (2000). Functionally significant secondary structure of the simian virus 40 late polyadenylation signal. Mol. Cell. Biol. *20*, 2926–2932.

Heeb, S., Blumer, C., and Haas, D. (2002). Regulatory RNA as mediator in GacA/RsmA-dependent global control of exoproduct formation in *Pseudomonas fluorescens* CHA0. J. Bacteriol. *184*, 1046–1056.

Hirata, H., Yoshiura, S., Ohtsuka, T., Bessho, Y., Harada, T., Yoshikawa, K., and Kageyama, R. (2002). Oscillatory expression of the bHLH factor Hes1 regulated by a negative feedback loop. Science *298*, 840–843.

Ibba, M., and Söll, D. (2000). Aminoacyl-tRNA synthesis. Annu. Rev. Biochem. *69*, 617–650.

Jeong, E.J., Hwang, G.S., Kim, K.H., Kim, M.J., Kim, S., and Kim, K.S. (2000). Structural analysis of multifunctional peptide motifs in human bifunctional tRNA synthetase: identification of RNA-binding residues and functional implications for tandem repeats. Biochemistry *39*, 15775–15782.

Jia, J., Arif, A., Ray, P.S., and Fox, P.L. (2008). WHEP domains direct noncanonical function of glutamyl-Prolyl tRNA synthetase in translational control of gene expression. Mol. Cell *29*, 679–690.

Jordheim, L.P., Sève, P., Trédan, O., and Dumontet, C. (2011). The ribonucleotide reductase large subunit (RRM1) as a predictive factor in patients with cancer. Lancet Oncol. *12*, 693–702.

Kamba, T., and McDonald, D.M. (2007). Mechanisms of adverse effects of anti-VEGF therapy for cancer. Br. J. Cancer *96*, 1788–1795.

Kapasi, P., Chaudhuri, S., Vyas, K., Baus, D., Komar, A.A., Fox, P.L., Merrick, W.C., and Mazumder, B. (2007). L13a blocks 48S assembly: role of a general initiation factor in mRNA-specific translational control. Mol. Cell *25*, 113–126.

Karres, J.S., Hilgers, V., Carrera, I., Treisman, J., and Cohen, S.M. (2007). The conserved microRNA miR-8 tunes atrophin levels to prevent neurodegeneration in Drosophila. Cell *131*, 136–145.

Kyriacou, S.V., and Deutscher, M.P. (2008). An important role for the multienzyme aminoacyl-tRNA synthetase complex in mammalian translation and cell growth. Mol. Cell *29*, 419–427.

Leung, A.K., and Sharp, P.A. (2010). MicroRNA functions in stress responses. Mol. Cell *40*, 205–215.

Licatalosi, D.D., and Darnell, R.B. (2010). RNA processing and its regulation: global insights into biological networks. Nat. Rev. Genet. *11*, 75–87.

Mayr, C., and Bartel, D.P. (2009). Widespread shortening of 3'UTRs by alternative cleavage and polyadenylation activates oncogenes in cancer cells. Cell *138*, 673–684.

Mazumder, B., and Fox, P.L. (1999). Delayed translational silencing of ceruloplasmin transcript in gamma interferon-activated U937 monocytic cells: role of the 3′ untranslated region. Mol. Cell. Biol. *19*, 6898–6905.

Mazumder, B., Sampath, P., Seshadri, V., Maitra, R.K., DiCorleto, P.E., and Fox, P.L. (2003). Regulated release of L13a from the 60S ribosomal subunit as a mechanism of transcript-specific translational control. Cell *115*, 187–198.

Mazumder, B., Seshadri, V., Imataka, H., Sonenberg, N., and Fox, P.L. (2001). Translational silencing of ceruloplasmin requires the essential elements of mRNA circularization: poly(A) tail, poly(A)-binding protein, and eukaryotic translation initiation factor 4G. Mol. Cell. Biol. *21*, 6440–6449.

McMahon, K.W., Hirsch, B.A., and MacDonald, C.C. (2006). Differences in polyadenylation site choice between somatic and male germ cells. BMC Mol. Biol. *7*, 35.

Millevoi, S., and Vagner, S. (2010). Molecular mechanisms of eukaryotic pre-mRNA 3′ end processing regulation. Nucleic Acids Res. *38*, 2757–2774.

Mukhopadhyay, R., Ray, P.S., Arif, A., Brady, A.K., Kinter, M., and Fox, P.L. (2008). DAPK-ZIPK-L13a axis constitutes a negative-feedback module regulating inflammatory gene expression. Mol. Cell *32*, 371–382.

Mukhopadhyay, R., Jia, J., Arif, A., Ray, P.S., and Fox, P.L. (2009). The GAIT system: a gatekeeper of inflammatory gene expression. Trends Biochem. Sci. *34*, 324–331.

Park, S.G., Schimmel, P., and Kim, S. (2008). Aminoacyl tRNA synthetases and their connections to disease. Proc. Natl. Acad. Sci. USA *105*, 11043–11049.

Ray, P.S., and Fox, P.L. (2007). A post-transcriptional pathway represses monocyte VEGF-A expression and angiogenic activity. EMBO J. *26*, 3360–3372.

Ray, P.S., Jia, J., Yao, P., Majumder, M., Hatzoglou, M., and Fox, P.L. (2009). A stress-responsive RNA switch regulates VEGFA expression. Nature *457*, 915–919.

Ray, P.S., Sullivan, J.C., Jia, J., Francis, J., Finnerty, J.R., and Fox, P.L. (2011). Evolution of function of a fused metazoan tRNA synthetase. Mol. Biol. Evol. *28*, 437–447.

Ribas de Pouplana, L., and Schimmel, P. (2001). Aminoacyl-tRNA synthetases: potential markers of genetic code development. Trends Biochem. Sci. *26*, 591–596.

Sampath, P., Mazumder, B., Seshadri, V., and Fox, P.L. (2003). Transcript-selective translational silencing by gamma interferon is directed by a novel structural element in the ceruloplasmin mRNA 3′ untranslated region. Mol. Cell. Biol. *23*, 1509–1519.

Sampath, P., Mazumder, B., Seshadri, V., Gerber, C.A., Chavatte, L., Kinter, M., Ting, S.M., Dignam, J.D., Kim, S., Driscoll, D.M., and Fox, P.L. (2004). Noncanonical function of glutamyl-prolyl-tRNA synthetase: gene-specific silencing of translation. Cell *119*, 195–208.

Sassone-Corsi, P., Sisson, J.C., and Verma, I.M. (1988). Transcriptional autoregulation of the proto-oncogene fos. Nature *334*, 314–319.

Stockmann, C., Doedens, A., Weidemann, A., Zhang, N., Takeda, N., Greenberg, J.I., Cheresh, D.A., and Johnson, R.S. (2008). Deletion of vascular endothelial growth factor in myeloid cells accelerates tumorigenesis. Nature *456*, 814–818.

Tammela, T., Enholm, B., Alitalo, K., and Paavonen, K. (2005). The biology of vascular endothelial growth factors. Cardiovasc. Res. *65*, 550–563.

van Hoof, A., Frischmeyer, P.A., Dietz, H.C., and Parker, R. (2002). Exosome-mediated recognition and degradation of mRNAs lacking a termination codon. Science *295*, 2262–2264.

Wakasugi, K., and Schimmel, P. (1999). Two distinct cytokines released from a human aminoacyl-tRNA synthetase. Science *284*, 147–151.

Wakasugi, K., Slike, B.M., Hood, J., Otani, A., Ewalt, K.L., Friedlander, M., Cheresh, D.A., and Schimmel, P. (2002). A human aminoacyl-tRNA synthetase as a regulator of angiogenesis. Proc. Natl. Acad. Sci. USA *99*, 173–177.

Wu, C., and Alwine, J.C. (2004). Secondary structure as a functional feature in the downstream region of mammalian polyadenylation signals. Mol. Cell. Biol. *24*, 2789–2796.

EXTENDED EXPERIMENTAL PROCEDURES

Reagents and Antibodies

Restriction enzymes, Taq DNA polymerase, and protein and DNA ladders were purchased from Fermentas (Hanover, MD, USA). Yeast tRNA and RNase inhibitor were from Ambion (Austin, TX, USA) and phospho-safe extraction reagent from Novagen (Madison, WI, USA). Rabbit reticulocyte lysate, pGEM-T vector system, large-scale RNA production system-T7, and dual Luciferase reporter assay system were obtained from Promega (Madison, WI, USA). Protease inhibitor cocktail was from Roche, human interferon (IFN)-γ from R&D Systems (Minneapolis, MN, USA), human monocyte nucleofector kit from Lonza (Basel), and synthetic morpholino oligos from Gene Tools (Philomath, OR, USA). Reagents for protein purification, nuclear and cytoplasmic extraction, and immunoanalysis were from Pierce (Rockford, IL, USA) and BioRad (Hercules, CA, USA). Protein A/G beads, anti-VEGF-A antibody, and antibodies against N and C termini of RRM1 were from Santa Cruz (Santa Cruz, CA, USA). Primers, dNTP mix, TRIzol LS reagent, one-step RT-PCR system, and competent cells were purchased from Invitrogen (Carlsbad, CA, USA). Anti-rabbit IgG, anti-mouse IgG, and random primer labeling kit were from GE healthcare (Chalfont St. Giles, UK). Translation grade [^{35}S]methionine was from NEN-Dupont (Boston, MA, USA), and γ-[^{32}P]UTP and α-[^{32}P]CTP from PerkinElmer (Boston, MA, USA). Anti-EPRS linker antibody was generated as described (Ray et al., 2009). Anti-N-terminus EPRS antibody was from Abcam (Cambridge, MA, USA). Anti-PRS antibody was a generous gift from Dr. David Dignam. Anti-LysRS antibody was from Bethyl (Montgomery, TX, USA), anti-NSAP1 antibody from AnaSpec (Fremont, CA, USA), anti-c-Myc and anti-L13a antibodies from Cell Signaling (Danvers, MA, USA), and mouse and rabbit anti-CPSF100 antibody and other reagents were from Sigma-Aldrich (St. Louis, MO, USA). Anti-β-actin antibody was from Biovision (CA).

Cell Culture

Human U937 monocytic cells (ATCC, Rockville, MD, USA) and primary human PBM (from healthy clinical donors) were cultured in RPMI 1640 medium containing 10% fetal bovine serum (FBS). Human PBM were isolated by leukapheresis, followed by countercurrent centrifugal elutriation (Czerniecki et al., 1997), under a Cleveland Clinic Institutional Review Board-approved protocol that adhered to American Association of Blood Bank guidelines. For preparation of cytosolic extracts, the cells (10^7 cells per 10 ml) were incubated for 1 hr in medium containing 0.5% FBS and then incubated with IFN-γ (up to 500 units/ml) for an additional 8 or 24 hr. The cells were collected by centrifugation at low speed and cell lysates were prepared in phospho-safe extraction buffer containing protease inhibitor cocktail in ice.

Plasmids, Site-Directed Mutagenesis, and Recombinant Protein Expression

EPRS^{N1} (Met1 to Gln863) was cloned into pET-28 expression vector between SacI and SalI restriction sites and expressed as described (Jia et al., 2008). pcDNA3.1-EPRS^{N1}-c-Myc was generated using pET28-EPRS^{N1} as template and cloned between NotI and XbaI restriction sites. Primers used were as follows:

pET28-EPRS^{N1}-f(SacI): 5′-ATCGGAGCTCATGGCGACGCTCTCTCTGACC-3′
pET28-EPRS^{N1}-r(SalI): 5′-ACGCGTCGACTTACTGAGCCTTCAGGGACAGTAAG-3′
pcDNA3-EPRS^{N1}-f(NotI):
5′-ATAAGAATGCGGCCGCATGGCGACGCTCTCTCTGACC-3′
pcDNA3.1-EPRS^{N1}-r(XbaI): 5′-TGCTCTAGACTCTGAGCCTTCAGGGACAGTAAG-3′

The DNA template for in vitro transcription of EPRS^{N1} polyadenylation cassette RNA was cloned into PSP64 vector (PSP64-PAC) between SalI and EcoRI restriction sites. Primer sequences for cloning the entire polyadenylation cassette were as follows:

PAC-Forward (SalI): 5′-ACGCGTCGACATGAAGTTGCTGCACAAGGGGAGG-3′
PAC-Reverse (EcoRI): 5′-CCGGAATTCCTTTGTCAAAAAGTACTTTCGCTT-3′
Precleaved polyadenylation cassette reverse primer for cloning was (the forward primer is the same as PAC-Forward [SalI]):
5′-CCGGAATTCTACTGAGCCTTCAGGGACAG-3′

Specific mutations for EPRS^{N1} polyadenylation cassette RNA were introduced into PSP64-PAC by PCR-based mutagenesis. The reporter plasmids were constructed by subcloning polyadenylation cassettes into pRL-SV40 reporter plasmid between XbaI and BamHI sites. The SV40 polyadenylation cassette was replaced by EPRS^{N1} polyadenylation cassette within pRL-SV40 plasmid.

Immunoprecipitation and Immunodepletion

For immunoprecipitation, cell lysates (500 μl) prepared in phospho-safe extraction buffer were precleared with 50 μl protein A/G agarose beads at 4°C for 60 min. After centrifugation for 2 min at 4°C the supernatants were combined with 50 μl of protein A/G beads and 2 μg of antibody and incubated with rotation at 4°C for 4 hr. The beads were washed five times with 1 ml cold cell lysis buffer carefully removing all traces of the solution each time. Protein gel loading dye (100 μl) was added and the samples boiled before gel-loading. For immunodepletion, nuclear extracts from U937 cells were incubated with rabbit anti-CPSF100 antibody coupled

to protein A/G-agarose beads in extraction buffer. The beads were pelleted, the supernatants subjected to two additional rounds of depletion, and immunodepletion established by immunoblot with mouse anti-CPSF100 antibody.

Metabolic Labeling

U937 cells (10^7 cells in 4 ml of RPMI 1640 medium) were treated with IFN-γ (0 to 500 U/ml) for 8 or 24 hr. The cells were collected by centrifugation, suspended, and metabolically labeled for 1 hr with [^{35}S]methionine (100 mCi/ml) in methionine-free RPMI 1640 medium. The cells were collected by centrifugation and lysed with phospho-safe extraction buffer containing protease inhibitor cocktail. Newly synthesized, ^{35}S-labeled ZIPK was immunoprecipitated from lysates using rabbit anti-human ZIPK antibody (AbD Serotec) and protein A/G-agarose in cell lysis buffer. Proteins were resolved by 10% SDS-PAGE, and the gel was dried and applied to phospho-screen for analysis.

RNA Blot Analysis

For RNA blot analysis, total RNA was extracted from 10^8 U937 cells using Trizol reagent according to the manufacturer's instructions. RNA (20 μg) was fractionated on 1% agarose-formaldehyde gel and transferred to Zeta-Probe GT membrane (Bio-rad). The blot was hybridized with the random primer-labeled cDNA probe, and the signal scanned and quantified by Phosphoimager. The blot was then stripped and rehybridized with the other cDNA probe. ERS-specific probe is a random primer-labeled 1012 bp cDNA probe (nucleotide positions 1734–2745 in the ORF covering ERS-C terminus-R1R2). PRS-specific probe is a random primer-labeled 1045 bp cDNA probe (nucleotide positions 2796–3850 in ORF covering R3-PRS-N-terminus). qRT-PCR determinations of *VEGF-A*, *Cp*, and *GAPDH* mRNA were done using the Taqman Gene Expression Assays for various targets and the StepOnePlus Real-Time PCR System (AB Applied Biosystems).

RIP-RT-PCR

U937 cell lysate (500 μg protein) was precleared by rotation with 100 μl of protein A/G-agarose beads for 1 hr at 4°C. The lysate was centrifuged at 1000 × g for 2 min and the supernatant incubated with 2 μg anti-c-Myc antibody at 4°C for 4 hr. The antibody-protein complex was incubated with 100 μl of protein A/G beads for 2 hr at 4°C; preimmune IgG was used as negative control. The beads were centrifuged briefly and washed five times by rotation with 0.5 ml lysis buffer at 4°C for 5 min. Immunoprecipitated RNA was extracted from the beads by Trizol method. Total RNA was extracted from the lysate as a positive control for RT-PCR. Immunoprecipitated RNA (3 μl) and total RNA (1 μg) were subjected to RT-PCR using Taq DNA polymerase, and the PCR product visualized by 1.5% agarose gel electrophoresis.

Mass Spectrometry

Proteins immunoprecipitated by anti-EPRS linker antibody from U937 cell lysates were resolved by 4%–20% SDS-PAGE gel. The 95 kDa, Coomassie-stained band was in-gel digested with trypsin and analyzed by capillary LC-MS/MS analysis (LTQ-linear ion trap MS system, ThermoFinnigan, San Jose, CA, USA). CID spectra were queried against the human reference sequence database using Mascot software, and matching spectra verified manually and by using the Sequest and Blast as needed.

G/I Tailing and cDNA Cloning

Total RNA (10 μg) from U937 cells was extracted with Trizol reagent and subjected to G/I tailing following the protocol from Poly(A) Tail-Length Assay Kit (Affymetrix). Poly(G/I)-tailed RNA product was subjected to RT-PCR by using oligo-dC primer. The cDNA obtained from reverse transcription was used as template for both poly(A)-tailed cDNA PCR and gene-specific PCR. The forward primer for both PCR reactions was 5′-ATGAAGTTGCTGCACAAGGGGAGG-3′. The reverse primers for poly(A)-tailed cDNA and gene-specific PCR were oligo-dC and 5′-TACTGAGCCTTCAGGGACAGTAA-3′, respectively. The reaction products were loaded onto a 2.5% agarose TBE gel. The band with lowest molecular weight was removed, purified, and ligated into pGEM-T vector for DNA sequencing.

Polysome Profiling

U937 Cells (10^7) were preincubated with cycloheximide (CHX, 100 μg/ml) for 15 min and washed twice with CHX-containing cold PBS. Cells were suspended in 350 μl TMK lysis buffer (10 mM, pH 7.4 Tris-Cl, 5 mM $MgCl_2$, 100 mM KCl, 1% [v/v] Triton X-100, 0.5% [w/v] deoxycholate, 1 U/ml RNase inhibitor, 2 mM DTT, and 100 μg/ml CHX) and incubated on ice for 5 min. The lysates were centrifuged at 12,000 rpm for 10 min and the supernatant collected. Sucrose gradient solutions (10% or 50% sucrose [w/v], 20 mM, pH 7.4 HEPES, 100 mM KCl, 5 mM $MgCl_2$, 2 mM DTT) containing 80 U RNase inhibitor and 100 μg/ml CHX were freshly prepared and kept at 4°C. The cytosolic lysates were loaded on the sucrose gradient, centrifuged at 29,000 rpm for 4 hr and subjected to gradient fractionation (Teledyne-Isco). Eight tubes of 1 ml fractions were collected including light mRNP fraction, 40S, 60S, 80S (translationally inactive pool) and heavy polysome fractions (translationally active pool).

In Vitro Translation

Capped, poly(A)-tailed template mRNAs were prepared using mMESSAGE mMACHINE SP6 or T7 kits (Ambion). FLuc-VEGF-A GAIT element-poly(A) (200 ng) and RLuc (200 ng) reporter RNAs were incubated with IFN-γ treated U937 cytosolic extract (500 ng protein)

in the presence of rabbit reticulocyte lysate, [^{35}S]methionine, 1 mM amino acid mix without methionine, and 40 U RNase inhibitor for 90 min at 30°C. The translation products were added with loading dye, boiled at 95°C for 3 min, and resolved by 10% SDS-PAGE. The gel was dried, applied to the phospho-screen overnight, and visualized by Phosphorimager.

RNA-Protein Interaction by SPR

Protein binding to *Cp* GAIT-element RNA was determined by SPR in a Biacore 3000 system (Jia et al., 2008). 0.2 μM biotinylated, wild-type, and mutant GAIT-element RNA (U87C) were separately immobilized on an SA streptavidin sensor chip in HBS-P buffer containing 0.01 M HEPES (pH 7.4), 0.15 M NaCl, 0.005% v/v surfactant P20, and 5% glycerol according to manufacturer's instructions. The sensor chip was primed for 6.5 min and prewashed three times with wash buffer (1 M NaCl, 50 mM NaOH) at 30 μl/min for 1 min. The analyte flow rate was 5 μl/min in the same HBS-P buffer containing 5 mM $MgCl_2$. Sensorgrame was run on the flow path of Fc1, Fc2, and Fc3 for reference control, wild-type GAIT-element RNA, and mutant GAIT-element RNA (U87C), respectively. Flow cells were regenerated with three rinses of 1 M NaCl at 30 μl/min. Dissociation constants were calculated for a range of protein concentrations using Biaevaluation software (Biacore).

In Vitro Cleavage and Polyadenylation Assays

PSP64-PAC vector was linearized by EcoRI digestion, and the polyadenylation cassette RNA was transcribed using MAXIscript SP6 in vitro transcription kit (Ambion). Transcribed RNA was dephosphorylated with CIP at 37°C for 30 min, and CIP removed by phenol/chloroform extraction. The RNA product was 5′-end labeled with ^{32}P-γ-ATP catalyzed by polynucleotide kinase at 37°C for 1 hr, and purified using a Micro Bio-Spin 30 chromatography column; the purity was tested by 8 M urea-5% polyacrylamide gel. To measure the cleavage reaction, ^{32}P-labeled polyadenylation cassette RNA (1 nM, 10,000 cpm/μl) was incubated with U937 nuclear extract (50%, v/v), KCl (50 mM), $MgCl_2$ (1 mM), EDTA (0.1 mM), glycerol (10%), DTT (0.2 mM), creatine phosphate (20 mM), and polyvinyl alcohol (2%). Precleaved polyadenylation cassette RNA was in vitro transcribed from PCR-generated template amplified from wild-type plasmid PSP64-PAC or its mutant using the following primers:

SP6 primer: 5′-TATTTAGGTGACACTATAG-3′
Reverse primer: 5′-TACTGAGCCTTCAGGGACAG-3′

For in vitro polyadenylation assay, 1 mM ATP was added to the same reaction solution in the presence of precleaved polyadenylation cassette RNA.

Cell Transfection and Dual Luciferase Reporter Assay

To measure polyadenylation-based translation efficiency of chimeric Luc constructs, U937 cells (10^7) were transiently transfected with 0.5 μg pRL-SV40 plasmid (containing polyadenylation cassette) with the human monocyte nucleofector kit. To monitor transfection efficiency, cells were cotransfected with 1 μg pCD-FLuc (CMV-FLuc) plasmid. The cells were electroporated in a 4 mm gap cuvette, allowed to recover for 24 hr in RPMI 1640 medium containing 10% FBS, and then treated with IFN-γ in medium containing 0.5% FBS. Treated cells were washed twice with PBS, and FLuc and RLuc activities in cell extracts measured by chemiluminescence using Dual Luciferase Reporter system (Promega). RLuc activity was normalized by FLuc activity. To knock down endogenous $EPRS^{N1}$, U937 cells were transfected with morpholino antisense oligomer (5′-CCCAGTTTTTTCTTTATACT GAGCC-3′) or a control morpholino oligomer using human monocyte nucleofector kit.

Nested RT-PCR and RNA Blot for Detecting Candidate PAY*-Derived mRNAs

Total RNA was extracted from U937 cells and subjected to reverse transcription by using oligo-dT primer. Two-round nested PCR was performed with the cDNA as template. In the first round PCR, anchored oligo-dT was used as the reverse primer, and the forward primers were as follows:

ANKRD32-f500: 5′-ACTAACCAAGGACTATATAATTCA-3′
SYCP1-f500: 5′-CTGCCAGCCGCCCGGGGCCCACGC-3′
COL2A1-f500: 5′-CTCCTGGAGCCCCTGGGCCCCCTG-3′
GBA2-f500: 5′-AGGTGTGGCAGGATCTACTTCAGGATGGACAGCT-3′
ZDHHC6-f500: 5′-ATGACGGAGTCATCCAAGGAGGAA-3′
MFGE8-f500: 5′-GACCTTCTTGGGTTTGCAGCATTG-3′
RRM1-f500: 5′-TTCCTTGATTTAAAGAAGAACACA-3′

In the second round PCR, anchored oligo-dT was used as the reverse primer, and forward primers were as follows:

ANKRD32-f200: 5′-AAGCTGAGAAAGAAAAAGATAACT-3′
SYCP1-f200: 5′-ATGATTTTGAGTTTCCATTTGCAA-3′
COL2A1-f200: 5′-TGGCAAAGATGGTGCTAATGGAAT-3′
GBA2-f200: 5′-TATTGGATGACAGATCACTG CCTG-3′

ZDHHC6-f200: 5′-CAAAATGGGTACGTTCTGTTCGGT-3′
MFGE8-f200: 5′-TGTTTGAGACCCCTGTGGAGGCTC-3′
RRM1-f200: 5′-GAGCAACCAGCAGAACCTGGGAAC-3′

The positive control primers for expression of full-length mRNAs included the forward primers used in the second round PCR and the following reverse primers:

ANKRD32-r: 5′-TATACATGGTCTCTCTTAAGGCAC-3′
SYCP1-r: 5′-CCTTATACAGTTTTGAATACACTC-3′
COL2A1-r: 5′-CGGCCCGCATGTACTGCAGGGGGT-3′
GBA2-r: 5′-ACATGCGGTACTCCTGGCCCTCAA-3′
ZDHHC6-r: 5′-AGAATCATGACAGTCCAATTTATC-3′
MFGE8-r: 5′-GAAGAGATGCAAGCCCCAGGTCTT-3′
RRM1-r: 5′-AATTTTATTCAAGTTTCGGACAAC-3′

Primers for preparing the ^{32}P-α-CTP internal-labeled, N terminus-specific cDNA probes for northern blot analysis of RRM1 are RRM1-f500 and RRM1-r shown above. Primers for C terminus-specific cDNA probes for RNA blot analysis of RRM1 are as follows:

RRM1-Fc: 5′-GTACCAGAGGCATGCCTATCAAATA-3′
RRM1-Rc: 5′-CATGCAATAATCTGGTTTTTCATCT-3′

Modeling Procedures

Overview

We developed a mathematical model to elucidate the mechanism or component leading to the apparent saturation dynamics obtained after translational silencing at 24 hr (Figure 1B). An initial dynamic model (Figure 2A, left, without dashed compartment and vectors) of the GAIT-mediated translational inhibition was developed to simulate the experimental finding of the translational trickle observed at 24 hr. This model, however, failed to simulate the experimental data regardless of the model parameter values. A putative GEIF was introduced to protect a small amount of mRNA from GAIT pathway inhibition. This enhanced model with GEIF (Figure 2A, with dashed compartment and vectors) could simulate the experimental data and explain the translational trickle mechanism, which led to experimental identification of EPRS^{N1} and consequent transcriptome expansion. In addition to the initial model, we examined two other models that failed to simulate the nonlinear translational trickle at 24 hr. One model included a GAIT complex inhibitor that sequesters the complex, preventing binding to GAIT target mRNAs (Figure S1A). The second model included two pools of mRNA, with and without GAIT element (Figure S1E). Among the various models that we tried, only the enhanced model with GEIF yielded the appropriate response associated with the observed trickle.

Model Components and Expected Behavior

In our model, the four GAIT proteins (EPRS, NSAP1, L13a, and GAPDH) are lumped into a "GAIT complex." G_i represents separate unassembled or partially assembled GAIT component proteins present before 14 hr and after 32 hr, and hence without any translational silencing activity. The GAIT complex stoichiometry is represented by IFN-γ-induced released EPRS (as well as free L13a), which is approximately 50% of tRNA multisynthetase complex (Sampath et al., 2004). The GAIT complex is in excess compared to GAIT-element-bearing target mRNA, *M*. The amount of GAIT target mRNA was determined by ribonucleoprotein immunoprecipitation assay (unpublished data). The amount of GAIT complex was estimated from reported amount of tRNA multisynthetase complex in human cells (David et al., 2011). This indicated that the stoichiometry ratio of GAIT complex to target mRNA is in the range of 50–100. *GM* is the silenced, GAIT-bound mRNA that cannot undergo translation. *FM* is the GEIF-bound mRNA that can undergo translation to form the GAIT target protein *P*. After an IFN-γ bolus, activation of GAIT complex is delayed by 14 hr. Negative regulation by feedback inhibition of DAPK and ZIPK proteins (which are GAIT pathway target proteins) suppresses L13a phosphorylation that causes the GAIT complex to disassemble into G_i so that $G = 0$ after 32 hr (Mukhopadhyay et al., 2008).

Kinetic Processes

The reaction kinetics from 0 to 24 hr after IFN-γ treatment of myeloid cells are described here. There is a transcriptional surge in the synthesis of GAIT-element-bearing mRNA, *M*, when the cells are stimulated with an initial bolus of IFN-γ, $IFN\gamma_0$.

$$M \xrightarrow[k_{IFN}]{IFN\gamma_0} nM \tag{1}$$

where *n* is a positive number indicating the extent of transcriptional surge in mRNA production, and k_{IFN} is the associated rate constant. The rate of the transcriptional surge is defined in the input rate section below. IFN-γ treatment of cells also triggers the cascade inducing delayed activation of GAIT complex. GAIT complex can bind the 3′ UTR of the native GAIT-element-bearing mRNA to form the mRNA-GAIT protein complex, *GM* leading to translational inhibition.

$$G + M \underset{k'_{GM}}{\overset{k_{GM}}{\rightleftharpoons}} GM. \tag{2}$$

k_{GM} and k'_{GM} are the forward and reverse reaction rate constants. We assumed that GEIF (F) binds to M:

$$F + M \underset{k'_{FM}}{\overset{k_{FM}}{\rightleftharpoons}} FM \tag{3}$$

where k_{FM} and k'_{FM} are the forward and reverse reaction rate constants, respectively. Assume that a sequestering protein/complex or decoy RNA were available. Then the GAIT complex could be sequestered in the presence of such an inhibitor I that inhibits GAIT repression:

$$G + I \underset{k'_{GI}}{\overset{k_{GI}}{\rightleftharpoons}} GI \tag{4}$$

where k_{GI} and k'_{GI} are the forward and reverse reaction rate constants, respectively. The GAIT pathway regulated protein, P, may be generated by the active mRNA templates (M, FM, M_w) with a translation rate constant k_P. Here, M_w represents any mRNA transcripts lacking GAIT element, which could be generated by alternative splicing or polyadenylation. In this way, there could be protection from GAIT-mediated silencing.

$$\left.\begin{matrix} M \\ FM \\ M_w \end{matrix}\right\} \overset{k_P}{\rightarrow} P. \tag{5}$$

Dynamic Equations

The total GAIT complex (unbound, G, mRNA-bound, GM, inhibitor-bound, GI) and total GEIF (unbound, F, and mRNA-bound, FM) remain constant at their respective initial values (G_0, F_0). Furthermore, there is no reason for the total inhibitor to change, so that total inhibitor remains constant at its initial value I_0. The following dynamic relationships exist:

$$F = F_0 - FM \Rightarrow \frac{dF}{dt} = -\frac{dFM}{dt} \tag{6}$$

$$G = G_0 - GM - GI \Rightarrow \frac{dG}{dt} = -\frac{dGM}{dt} - \frac{dGI}{dt} \tag{7}$$

$$I = I_0 - GI \Rightarrow \frac{dI}{dt} = -\frac{dGI}{dt}. \tag{8}$$

For this system, the independent state variables change according to the following dynamic mass balance equations:

$$\frac{dM}{dt} = R_{M_{IFN\gamma}} - k_{GM}[M][G] + k'_{GM}[GM] - k_{FM}[M][F] + k'_{FM}[FM] \tag{9}$$

where $R_{M_{IFN\gamma}}$ is the input rate.

$$\frac{dGM}{dt} = k_{GM}[M][G] - k'_{GM}[GM] \tag{10}$$

$$\frac{dFM}{dt} = k_{FM}[M][F] - k'_{FM}[FM] \tag{11}$$

$$\frac{dGI}{dt} = k_{GI}[G][I] - k'_{GI}[GI] \tag{12}$$

$$\frac{dP}{dt} = k_P[M + FM + M_w]. \tag{13}$$

The effective model output rate is $R_P = \alpha_P k_P[M + FM + M_w]$, where α_p is a calibration coefficient related to the rate of protein synthesis. The reverse reaction rate constants are expressed in terms of dissociation constants $(k'_{GM} = K_{D_{GM}} k_{GM};\ k'_{FM} = K_{D_{FM}} k_{FM};\ k'_{GI} = K_{D_{GI}} k_{GI})$. The initial conditions for the different species are indicated in Table S1.

Input Rate

The input rate represents the transcriptional surge in GAIT-element-bearing mRNA as a result of an IFN-γ input bolus (in the absence of active G and F). From the total GAIT-element-bearing mRNA $(TM(t))$ measurements that incorporate this transcriptional surge, one can estimate the input rate. The mRNA pool lacking GAIT element $(M_w(t))$ is assumed to be directly proportional to the total GAIT-element-bearing mRNA $(TM(t))$:

$$M_w(t) = \frac{TM(t)}{R_{M/M_w}} \tag{14}$$

where R_{M/M_w} is proportionality constant representing the ratio of total GAIT-element-bearing mRNA to the mRNA pool lacking the GAIT element. The time course of total GAIT-element-bearing mRNA can be described by a function that has an early linear increase and then reaches a maximum value:

$$TM(t) = TM_{\max}[1 - \exp(-k_{IFN} t)] \tag{15}$$

Experimental data of total GAIT-element-bearing mRNA measurement as a function of $IFN\gamma_0$ indicates a saturation expression for the steady-state total GAIT-element-bearing mRNA levels $(TM_{\max})$ attained at 24 hr for various $IFN\gamma_0$ dosages.

$$TM_{\max} = \alpha_M \left(\frac{IFN\gamma_0}{K_M + IFN\gamma_0} \right) \tag{16}$$

where α_M is a coefficient related to total GAIT-element-bearing mRNA (as measured) and K_M is a parameter that characterizes the nonlinear relationship.

The input rate process is determined by differentiating $TM(t)$:

$$R_{M_{IFN\gamma}}(t) = \alpha_M k_{IFN} \left(\frac{IFN\gamma_0}{K_M + IFN\gamma_0} \right) \exp(-t k_{IFN}). \tag{17}$$

Model Simulations

After the $IFN\gamma_0$ bolus input, the GAIT complex is inactive for 14 hr as represented by G_i. Although the GAIT complex G becomes active, the total amount of GAIT complex is unchanged from its initial steady-state value, $G_{ss} = G_0$. It is active between 14 and 32 hr and then inactive after 32 hr according to the following conditions:

$$\begin{array}{l} 0 \le t \le 14:\ G_i = G_{ss},\ G(t) = 0,\ GM(t) = 0,\ GI(t) = 0 \\ 14 < t \le 32:\ G(t) = G_{ss} - GM(t) - GI(t),\ GM(t) > 0 \\ t > 32:\ G(t) = 0,\ G_i = G(32),\ GM(t) = GM_{SS} = GM(32) \end{array}.$$

We simulated following model variations:

(1) In the initial model without GEIF, we set

$$F(t) = 0,\ FM(t) = 0,\ I(t) = 0,\ GI(t) = 0,\ M_W(t) = 0,\ k_{FM} = 0,\ k'_{FM} = 0,\ k_{GI} = 0,\ k'_{GI} = 0$$

so that the model variables were limited to $M(t)$, $G(t)$, $GM(t)$. The initial model without GEIF was simulated with multiple values of G_{ss}.

(2) In the enhanced model with GEIF, we set

$$F(t) > 0,\ FM(t) > 0,\ k_{FM} > 0,\ k'_{FM} > 0,\ I(t) = 0,\ GI(t) = 0,\ M_W(t) = 0,\ k_{GI} = 0,\ k'_{GI} = 0$$

so that the model variables included $M(t)$, $G(t)$, $GM(t)$, $F(t)$, $FM(t)$.

(3) In the model with inhibitor that binds GAIT complex, we set

$$I(t) > 0,\ GI(t) > 0,\ k_{GI} > 0,\ k'_{GI} > 0,\ F(t) = 0,\ FM(t) = 0,\ M_w(t) = 0,\ k_{FM} = 0,\ k'_{FM} = 0$$

so that the model variables included $M(t)$, $G(t)$, $GM(t)$, $I(t)$, $GI(t)$.

(4) In the model with two pools of mRNA, we set

$$M_w(t) > 0,\ I(t) = 0,\ GI(t) = 0,\ k_{GI} = 0,\ k'_{GI} = 0,\ F(t) = 0,\ FM(t) = 0,\ k_{FM} = 0,\ k'_{FM} = 0$$

so that the model variables included $M(t)$, $G(t)$, $GM(t)$, $M_w(t)$.

Model Parameter Values

For all model simulations, parameter values were obtained directly or indirectly from experimental measurements by our laboratory or as reported by others (Table S2). A range of values was assumed for key parameters as specified below. Model simulations were performed under multiple conditions by solving the dynamic Equations (6)–(13) using an integrator for stiff, ordinary differential equations (ode15s, MATLAB, MathWorks). As specified below, some parameters were optimally estimated by a least-squares fit of model outputs to experimental data. These optimal estimates of the model parameters were obtained using nonlinear regression (lsqcurvefit, MATLAB, MathWorks).

For the function $TM_{\max}(IFN\gamma_0)$ of Equation (16), the parameter $K_M$was estimated initially as the value of $IFN\gamma_0$ at which the total mRNA reaches half of its maximal value from the data plot of $TM_{\max}$ versus $IFN\gamma_0$. Then, $\alpha_M$and K_M were estimated from the best fit of the model-predicted values of $TM_{\max}$ to its corresponding experimental values for all $IFN\gamma_0$ data. Subsequently, k_{IFN} was estimated from the best fit of the model-predicted values of $TM(t)$ using Equation (15) to its corresponding experimental values for all $IFN\gamma_0$ data. At a maximal $IFN\gamma_0$ bolus of 500 units/ml, we defined $M_{\max} = TM_{\max}(500)$, which is the experimentally measured steady-state value at 24 hr.

The initial model without GEIF was simulated with values of G_{ss} computed as the product $M_{\max}(G_{ss}/M_{\max})$ in which $M_{\max}$is determined as described above. In one case, the value of $(G_{ss}/M_{\max}) = 100$ as that reported in the literature (David et al., 2011 and unpublished data). In the second case, $(G_{ss}/M_{\max}) = 15$ as estimated by a least-squares fit of the model output to experimental data. This, however, is much less than the experimentally known range of $G_{ss}/M_{\max}$. For simulations with the GEIF-enhanced model as well as the model with inhibitor and the model with two pools of mRNA, we set $(G_{ss}/M_{\max}) = 100$, the value from literature. The model with inhibitor was simulated for multiple values of I_0. The model with two pools of mRNA was also simulated for a range of increasing fraction of M_w compared to the total GAIT-element-bearing mRNA reflecting a decrease in the ratio R_{M/M_w} of mRNA pool containing GAIT element to the mRNA pool devoid of GAIT element.

The rate constants for binding of GAIT complex to target mRNA $(k_{GM},\ k'_{GM} = K_{D_{GM}}\ k_{GM})$ were determined from SPR binding assays in the absence of GEIF. The forward rate constant for the binding of GEIF to target mRNA (k_{FM}) as well as binding of GAIT complex to inhibitor (k_{GI}) was assumed to be same as k_{GM}. Nonlinear regression with enhanced model with GEIF was used to estimate $K_{D_{FM}} = k'_{FM}/k_{FM}$, the dissociation constant for the binding of GEIF to the mRNA. The value of $K_{D_{GI}} = k'_{GI}/k_{GI}$ was varied from 0.1 to 1000 relative units to represent increasing affinity between the GAIT complex and inhibitor leading to increase in GAIT complex sequestering. The value of k_P was obtained from literature (Alon, 2007). Finally, with the GEIF-enhanced model, we simultaneously estimated $K_{D_{FM}}$, α_P, and F_0 by nonlinear regression.

Model Validation

Among the different models that we simulated, only the enhanced model with GEIF resulted in a nonlinear, saturation behavior at 24 hr after IFN-γ treatment. The reduction of GAIT complex achieved implicitly by varying the extent of GAIT compared to target mRNA in the initial model (Figure S1B), or explicitly by introducing an inhibitor for the GAIT complex silencing (Figures S1C and S1D) resulted in a linear behavior at 24 hr. Neither did the model containing two pools of mRNA (with and without the GAIT element) give the expected nonlinear trickle (Figure S1F).

The experimentally determined output rate $(R_{P_{\exp}})$ depends on the $IFN\gamma_0$ bolus, before and after translational inhibition (t = 8 and 24 hr, respectively). We compared the squared residuals $(R_{P_{\exp}} - R_p)^2$ with various $IFN\gamma_0$ inputs for the enhanced model with GEIF, the initial model with actual GAIT amount (100-fold excess) and the initial model with best-fit GAIT (15-fold excess) (Figure S1H). A criterion for the best-fitting model is minimum value of the sum of squared residuals, which was obtained for the enhanced model with GEIF. The lilliefors test (lillietest, MATLAB) revealed that the data were parametric. From a two-sample t test, we compared the model-predicted output, R_P, and experimental data, $R_{P_{\exp}}$. No statistical difference between these two outputs is characterized by $p > 0.05$, i.e., a good model fit. Only the enhanced model with GEIF for which p = 0.23 showed that there was no significant difference between the model output and experimental data, i.e., a good fit. With the other model, we found p = 0.002.

SUPPLEMENTAL REFERENCES

Alon, U. (2007). An Introduction to Systems Biology: Design Principles of Biological Circuits (Boca Raton, FL: Chapman and Hall/CRC).

David, A., Netzer, N., Strader, M.B., Das, S.R., Chen, C.Y., Gibbs, J., Pierre, P., Bennink, J.R., and Yewdell, J.W. (2011). RNA binding targets aminoacyl-tRNA synthetases to translating ribosomes. J. Biol. Chem. *286*, 20688–20700.

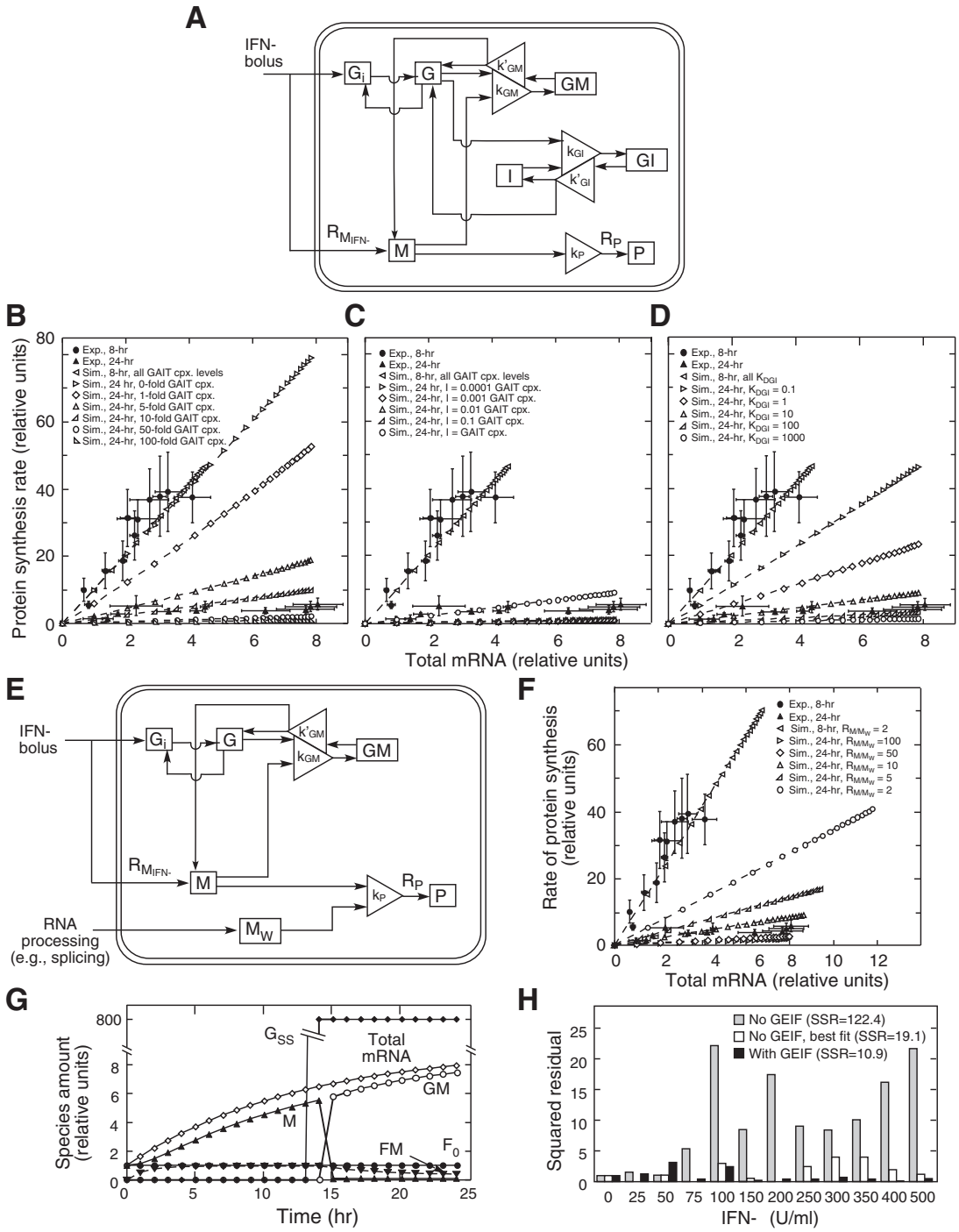

Figure S1. GAIT Complex Sequestration Model Development and Validation, Related to Figure 2

(A) Model with inhibitor (I) of GAIT-mediated repression bound to the GAIT complex (GI).

(B) Initial model without GEIF in which GAIT complex (cpx.) is varied with respect to target mRNA.

(C) Model with inhibitor with K_{DGI} fixed at 10 relative units and inhibitor concentration varied.

(D) Model with inhibitor with varied K_{DGI} (in relative units) and inhibitor concentration fixed equal to GAIT complex.

(E) Model with two mRNA pools with (M) and without (M_w) the GAIT element.

(F) Simulations with two pools of mRNA with ratio of GAIT-element-bearing to GAIT-element-lacking mRNA pool ($R_{M/MW}$) varied. The 8 hr trend line corresponds to $R_{M/MW}$ = 2, and all values of $R_{M/MW}$ > 2 gave trend lines with similar slope but decreasing lengths.

(G) Species dynamics in the GEIF-enhanced model following an IFN-γ bolus of 500 units/ml.

(H) Comparison of squared residuals. In parentheses are the sums of squared residuals (SSR).

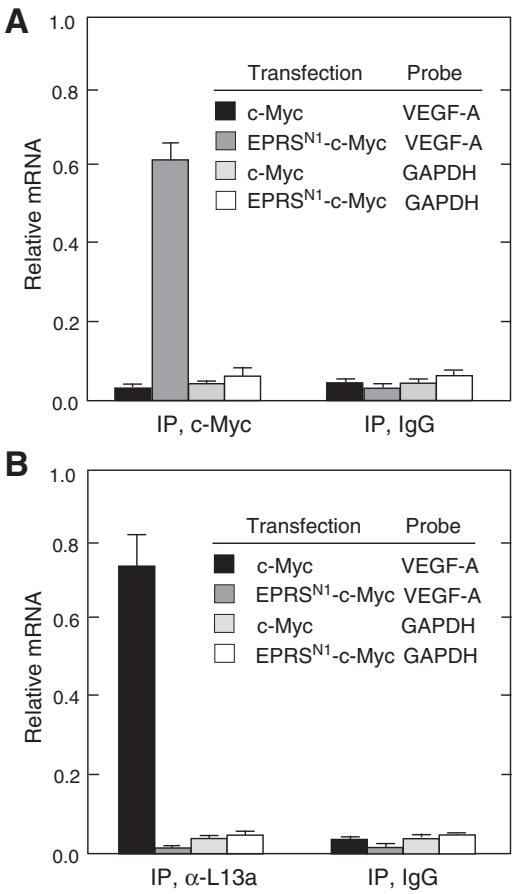

Figure S2. Analysis by qRT-PCR of EPRS^{N1} Binding to *VEGF-A* mRNA In Vivo, Related to Figure 5

(A) EPRS^{N1} interacts with *VEGF-A* mRNA in vivo. U937 cells were transfected with pcDNA3.1-EPRS^{N1}-c-Myc or c-Myc vector control, and lysates immunoprecipitated (IP) with anti-Myc antibody or IgG control. Extracted RNA was subjected to qRT-PCR using primers specific for *VEGF-A* or *GAPDH* mRNA and results normalized to input mRNA. Relative mRNA level was reported as mean ± SEM (n = 3).

(B) EPRS^{N1} inhibits GAIT complex binding to *VEGF-A* mRNA. U937 cells were transfected with pcDNA3.1-EPRS^{N1}-c-Myc or c-Myc vector control, and GAIT complex in lysates was immunoprecipitated with anti-L13a antibody or IgG control. Extracted RNA was subjected to qRT-PCR as in (A). Relative mRNA level was reported as mean ± SEM (n = 3).

A

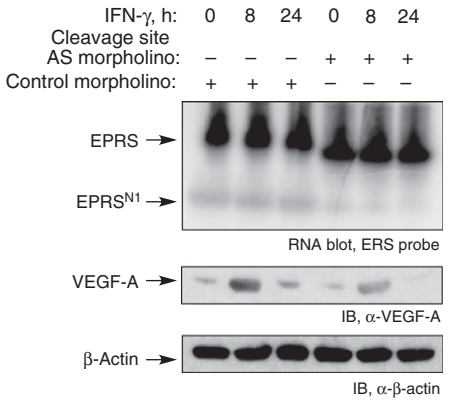

B

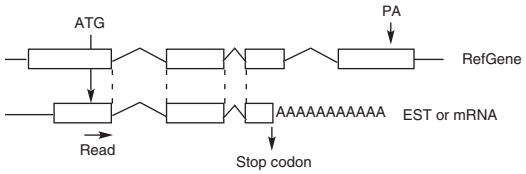

C

	mRNAs	ESTs
Total	899,946	8,301,471
Poly(A) transcript	64,586	615,997
Poly(A) transcript without internal priming	51,946	380,971
Poly(A) transcript assigned to RefGene	28,587	85,231
3' UTR-less in-CDS transcripts	28	63
RefGene-containing 3' UTR-less in-CDS transcripts	74	
PAY* candidate transcripts	7	

D

Gene	ResSeq ID	EST ID	UE, position	Cleavage sequence	DE	One exon	Function
ANKRD32	NM_032290	BC107571	AUUAAA, -207	UAU	–	No	Unknown
SYCP1	NM_003176	BC105299	–	UAU	–	–	DNA binding
COL2A1	NM_001844	BM682706	–	UAC	–	–	Inflammation
GBA2	NM_020944	BQ185158	–	UAU	–	–	Metabolism
ZDHHC6	NM_022494	AW139367	AUUAAA, -160	UAU	–	Yes	Transferase
MFGE8	NM_005928	AW205147, AW015751	AAUAAA, -267	UAU	–	No	Phagocytosis
RRM1	NM_001033	CA428666	AAUAAA, -18	UAC	–	Yes	DNA synthesis

Figure S3. Function of EPRS^{N1} in Human PBM and Global Detection of Candidate mRNAs Targeted by the PAY* Mechanism, Related to Figure 6

(A) Reduction of EPRS^{N1} expression inhibits the translational trickle of VEGF-A. Human PBM transfected with antisense morpholino oligomer targeting the cleavage site were treated with IFN-γ. *EPRS* and *EPRS^{N1}* mRNA were determined by RNA blot with ERS-specific probe, and VEGF-A and β-actin in cell lysates were determined by immunoblot.

(B) Schematic of detection method used to compare ESTs and mRNAs to human reference genes (RefGen) in University of California, Santa Cruz Genome Browser.

(C) Number of mRNAs and ESTs satisfying stepwise criteria for PAY* candidates.

(D) Conservation of upstream elements (UE), cleavage sequences, and downstream elements (DE), and cellular functions of PAY* candidates.

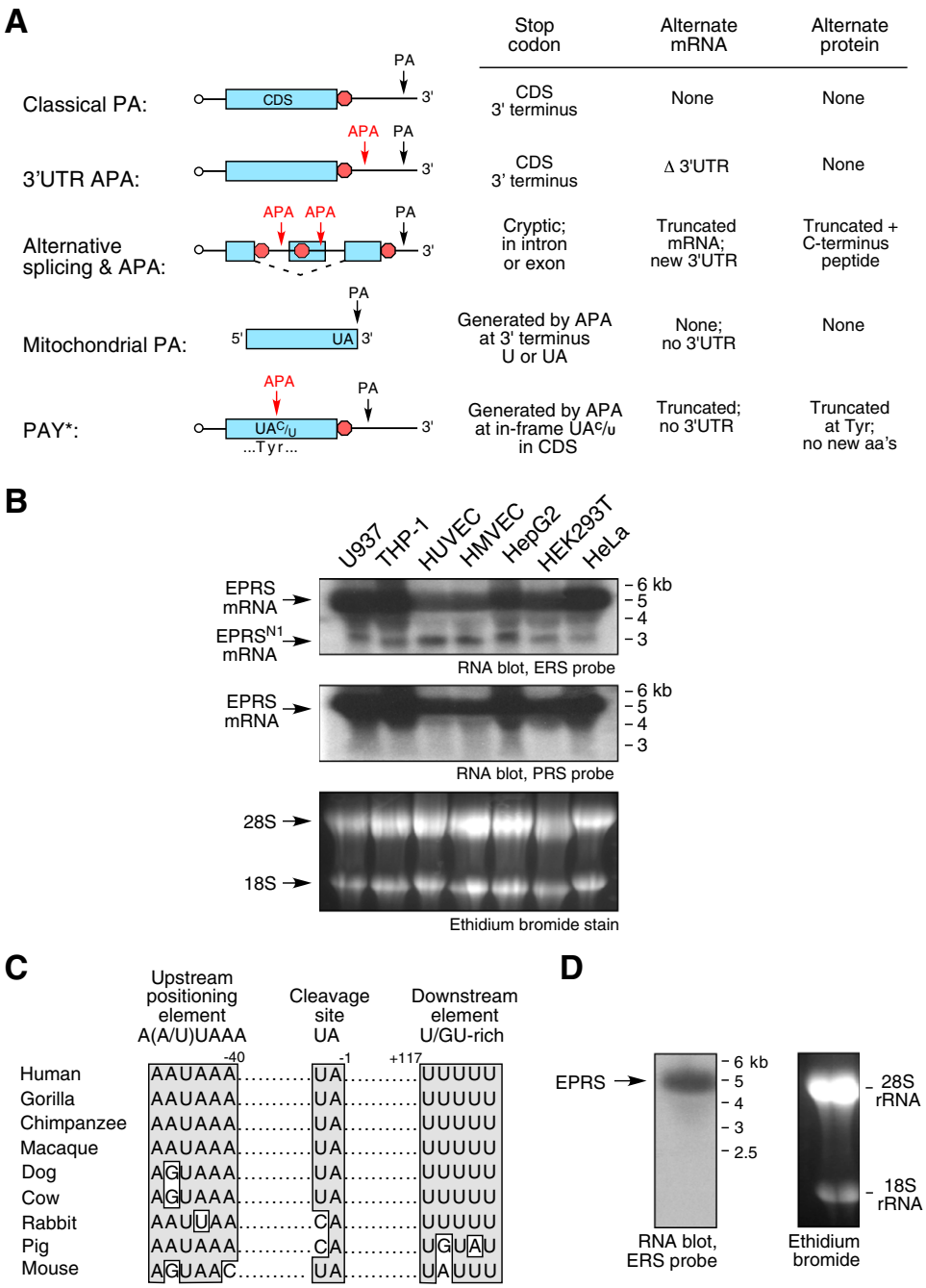

Figure S4. Comparison of PAY* to Other Types of Polyadenylation and Alternative Polyadenylation; Expression of EPRS^{N1} mRNA in Human Cells and Its Species Specificity, Related to Figure 7

(A) Schematic showing key sites and products of classical polyadenylation (PA) and four classes of alternative polyadenylation (APA) that generate protein-coding mRNAs. 5′ caps indicate by circles; stop codons indicated by red octagons.

(B) Total RNA was isolated from human myeloid U937 and THP-1 cells, human umbilical vein endothelial cells (HUVEC), human microvascular endothelial cells (HMVEC), and from human HepG2, HEK293T, and HeLa cells. RNA was was subjected to RNA blot analysis using ERS- and PRS-specific probes, and to ethidium bromide stain.

(C) Sequence alignment and conservation of polyadenylation elements in several mammalian species. Positions of upstream and downstream elements indicated for human EPRS^{N1}.

(D) Absence of mRNA encoding EPRS^{N1} in mouse RAW 264.7 cells.